AGU PUBLICATIONS

Water Resources Research

RESEARCH ARTICLE
10.1002/2015WR017316

Plant transpiration and groundwater dynamics in water-limited climates: Impacts of hydraulic redistribution

Xiangyu Luo[1,2], Xu Liang[1], and Jeen-Shang Lin[1]

[1]Department of Civil and Environmental Engineering, University of Pittsburgh, Pittsburgh, Pennsylvania, USA, [2]Now at Pacific Northwest National Laboratory, Richland, Washington, USA

Key Points:
- Mechanism of HR process is explored and explained via simulations using VIC+
- Effects of climates, vegetation, and soil types on HR process are assessed
- HR process promotes plant transpiration and modulates impacts of dry climates

Correspondence to:
X. Liang,
xuliang@pitt.edu

Citation:
Luo, X., X. Liang, and J.-S. Lin (2016), Plant transpiration and groundwater dynamics in water-limited climates: Impacts of hydraulic redistribution, *Water Resour. Res.*, *52*, 4416–4437, doi:10.1002/2015WR017316.

Received 3 APR 2015
Accepted 5 MAY 2016
Accepted article online 9 MAY 2016
Published online 10 JUN 2016

Abstract The role of groundwater in sustaining plant transpiration constitutes an important but not well-understood aspect of the interactions between groundwater, vegetation, the land surface, and the atmosphere. The effect of the hydraulic redistribution (HR) process by plant roots on the interplay between plant transpiration and groundwater dynamics under water-limited climates is investigated by using the Variable Infiltration Capacity Plus (VIC+) land surface model. Numerical experiments, with or without explicitly considering HR, are conducted on soil columns over a range of groundwater table depths (GWTDs) under different vegetative land covers, soil types, and precipitation conditions. When HR is not included, this study obtains transpiration–GWTD relationships consistent with those from watershed studies that do not include HR. When HR is included, the transpiration–GWTD relationships are modified. The modification introduced by HR is manifested in the soil moisture of the root zone. The mechanism of HR is explained by detailing the roles of the hydraulically redistributed water, the upward diffusion of soil water, and the daytime root uptake. We have found that HR is particularly important in water-limited climates under which plants have high transpiration demand. At the beginning stage of a dry period, HR modulates the severe impacts that climate has on plant transpiration. Only after a prolonged dry period, impacts of HR are lessened when the groundwater table drops below the depth of water uptake by roots and are diminished when plant transpiration is decoupled from groundwater dynamics.

1. Introduction

Water movement below the ground surface is an essential component of the hydrological cycle. Water flows in the unsaturated zone, the unconfined and confined aquifers. In this study, the term "groundwater" refers to water in the unconfined aquifer. Effects of groundwater on the land surface and atmospheric processes have received increasing attention in the large-scale hydrological and climate studies. As a result, the groundwater dynamics and groundwater–land surface interactions have been represented and investigated by some land surface and hydrological models [e.g., *Liang et al.*, 2003; *Chen and Hu*, 2004; *Maxwell and Miller*, 2005; *Yeh and Eltahir*, 2005; *Fan et al.*, 2007; *Niu et al.*, 2007]. Also, the groundwater component has been incorporated in some coupled land-atmosphere models and its role and impacts were explored [e.g., *Gutowski et al.*, 2002; *York et al.*, 2002; *Liang et al.*, 2006; *Miguez-Macho et al.*, 2007; *Leung et al.*, 2011; *Zampieri et al.*, 2012]. In addition, a three-dimensional groundwater flow model, coupled with a land surface model, has been used in studies to explore the surface and groundwater interactions and the impacts of spatial heterogeneities such as hydraulic conductivities and land cover types on the surface fluxes [e.g., *Maxwell and Miller*, 2005; *Maxwell*, 2010]. These studies demonstrated that groundwater dynamics played an important role in sustaining land surface water and energy fluxes, especially in water-limited climates and when the groundwater table was shallow. Through studies on watersheds, *Maxwell and Kollet* [2008], *Kollet and Maxwell* [2008], and *Condon et al.* [2013] showed that a pattern of a nonlinear relationship existed between annual mean evapotranspiration and the annual mean groundwater table depth (GWTD). This nonlinear relationship was described by a curve with two mildly sloped segments separated by a sharp sloped segment. The two mildly sloped segments indicate that the evapotranspiration is not sensitive to the GWTD when the groundwater table is either shallow or deep, while the steep segment indicates that evapotranspiration is sensitive to the change of the GWTD in-between the two GWTD regions. The discovery of the existence of such patterns between evapotranspiration and the GWTD sheds lights on the roles

of groundwater in land surface water and energy cycles. These patterns are further explored in the present study of the interaction of groundwater dynamics with plant transpiration in water-limited climates.

In the HR process, water moves via plant roots from soil of higher water potential to soil of lower water potential, in most circumstances from wet regions to dry regions. Thus, water can either move from the deep soil to the shallow soil (i.e., upward HR; also been referred to as "hydraulic lift") or from the shallow soil to the deep soil (i.e., downward HR; also been referred to as "hydraulic descent"). It has been verified by field experiments that HR exists for many plant species living under various climatic conditions [e.g., *Caldwell et al*., 1998; *Oliveira et al*., 2005; *Davis and Liang*, 2013].

Both experimental and modeling studies show that HR plays an important role in terrestrial water and energy cycles not only in the arid and semiarid regions [e.g., *Caldwell and Richards*, 1989; *Dawson*, 1993; *Ryel et al*., 2002] but also in regions experiencing distinct wet and dry seasons (e.g., the regions with Mediterranean-type climates) [e.g., *Lee et al*., 2005; *Wang*, 2011; *Luo et al*., 2013] by promoting dry-season transpiration and carbon assimilation [e.g., *Ryel et al*., 2002; *Lee et al*., 2005; *Amenu and Kumar*, 2008; *Wang*, 2011; *Luo et al*., 2013; *Quijano and Kumar*, 2015]. The modeling study of *Luo et al*. [2013] shows that the HR process affects the groundwater–land surface interactions by redistributing soil water in the root zone, while the experimental studies also reveal that HR can pump groundwater to the shallow soil at nighttime and provide additional transpiration water to trees [e.g., *Dawson*, 1996; *Lubczynski*, 2009]. These findings point to the necessity of including an adequate representation of HR, particularly in dry climates, in the land surface or hydrological models to assess impacts of the groundwater feedback to vegetation and to the surface fluxes. Its omission might have led to the conclusions that vegetative land cover had a limited impact on the land surface–subsurface interactions [*Rihani et al*., 2010]. Such conclusions have important consequences and warrant a fresh second look.

Although there are a few models that include both the HR process and the groundwater table, these models have important limitations in which either the groundwater dynamics or the HR process are not adequately accounted for, or the effects of HR on the interplay between groundwater and the land surface are not investigated in the context of major land-surface water and energy processes. For example, *Ryel et al*. [2002] use a conceptual HR representation when modeling soil water movement and soil water loss from transpiration. They prescribe a groundwater table, at a depth of 2.2 m, below the root zone and assume that the groundwater table does not fluctuate. *Mendel et al*. [2002] represent the HR process in their two-dimensional numerical model for water transport in the soil and the root system under idealized precipitation and transpiration conditions where the variable saturated flow in the soil is simulated. *Gou and Miller* [2014] consider deep-groundwater uptake and HR with the groundwater table kept at a constant depth of about 10 m below the surface.

Overall, in the context of the soil-plant-atmosphere continuum, studies on groundwater and surface water interactions considering the HR process have been limited [e.g., *Luo et al*., 2013]. In this study, we employ the VIC+ model [*Luo et al*., 2013] to investigate, in a comprehensive manner, the role of HR in the soil-plant-atmosphere continuum and how it interacts with the processes of groundwater dynamics, plant transpiration, upward diffusions, and other hydrological processes. The VIC+ model is an extension of the Three-Layer Variable Infiltration Capacity (VIC-3L) land surface model [*Liang et al*., 1994, 1996a, 1996b, 1999, 2003; *Cherkauer and Lettenmaier*, 1999; *Liang and Xie*, 2001; *Huang and Liang*, 2006]. It introduces and tightly integrates important biological and hydrological processes such as HR, photosynthesis, groundwater table dynamics, and plant water storage into the VIC-3L model. Moreover, the VIC+ model has been validated with analytical solutions and with observations from two AmeriFlux sites [*Luo et al*., 2013] and demonstrated to be a credible platform.

By employing the VIC+ model, we aim at systematically addressing the important issue of how HR, groundwater table (GWT) dynamics, and the upward diffusion interact, as well as how they affect plant transpiration and other water fluxes. Impacts of the plant water storage on transpiration and other fluxes are not investigated here as its influence on them is at the subdaily scale and not at the annual-scale investigated here. In this study, different numerical experiments, with and without the HR process, are conducted at a soil column for various circumstances in terms of groundwater table depths, vegetative land cover types, soil types, and precipitation conditions. More specifically, we analyze the following VIC+ modeling results with and without the HR process: (1) the relationships between GWTD and plant transpiration, (2) hydraulically redistributed water, (3) upward diffusion of soil water through a horizontal cross-section right below the root zone bottom, and (4) water uptake by roots during the daytime. The experiment design in this study enables us also to test the following hypothesis: "Plants modulate available soil water at the

beginning stage of a dry period through hydraulic redistribution by roots to tap moisture in the deeper soil layers or groundwater, and through stomatal response to maintain transpiration. However, when the GWT falls below a critical level, impacts of the dry period can be intensified and persist as plants and surface processes become decoupled from subsurface processes such that the reduction of plant transpiration is accelerated due to the significantly reduced soil moisture in the root zone." Here the surface processes include transpiration and HR; the subsurface processes include upward diffusion process and GWT dynamics. In this study, we define the beginning of a dry period to be at the time when plant transpiration is adequately less than its potential value controlled by the available energy.

The remainder of this paper is organized as follows: section 2 briefly reviews the VIC+ land surface model, with more focus on the features closely related to the purpose of this study. The setup of numerical experiments is described in section 3. Results and discussions are presented in section 4. Section 5 discusses the sensitivity due to temporal variation associated with the climate type. Conclusions are provided in section 6. Some technical details of the VIC+ model are also provided in an Appendix A.

2. VIC+ Land Surface Model

In an earlier study [*Luo et al*., 2013], the VIC+ land surface model was developed by extending the Three-Layer Variable Infiltration Capacity (VIC-3L) land surface model. The VIC-3L land surface model solves full energy and water budgets for the land surface and subsurface; it considers subgrid spatial variability of soil properties and precipitation [*Liang et al*., 1994, 1996a]; it accounts for both infiltration and saturation excess runoff generation mechanisms [*Liang and Xie*, 2001, 2003]; and it can simulate snow and frozen soil processes for cold climate conditions [e.g., *Cherkauer and Lettenmaier*, 1999, 2003]. Its unique capabilities of accounting for subgrid spatial variability in soil properties, precipitation, and runoff generation mechanisms make it less scale dependent, namely the simulated results are less sensitive to spatial scales, as compared to other land surface models [*Liang et al*., 1996a, 2004; *Li et al*., 2011].

In the early versions of the VIC-3L land surface model, the unconfined aquifer is not explicitly represented. It is lumped within the bottom soil layer from which the subsurface runoff (base flow) is estimated following the ARNO method [*Franchini and Pacciani*, 1991]. In the later version, the groundwater dynamics is explicitly represented using a moving boundary approach and the land surface and groundwater interactions are accounted for [*Liang et al*., 2003].

Luo et al. [2013] described, in detail, the concepts and equations of the VIC+ model and how the groundwater dynamics is tightly coupled with the HR process, photosynthesis process, plant water storage, and other VIC-3L processes. In VIC+, the groundwater dynamics is represented by an approach different from the previous version of VIC-3L model to facilitate incorporation of HR. In order for this paper to be self-contained, relevant basic concepts and main formulations are briefly summarized herein. The variably saturated flow in the soil is represented by a mixed form of the Richards equation:

$$\frac{\partial}{\partial z}\left[K_s \cdot \frac{\partial(\psi_s - \rho_w g z)}{\partial z}\right] - F_{sr} = \frac{\partial \theta}{\partial t} \tag{1}$$

where θ ($m^3\ m^{-3}$) is the volumetric soil water content; t is time; z (m) is the vertical coordinate originating from the ground surface; K_s ($m^2 \cdot s^{-1} \cdot Pa^{-1}$) is the soil hydraulic conductivity; ψ_s (Pa) is the soil water potential; ρ_w ($kg \cdot m^{-3}$) is the water density; g ($m \cdot s^{-2}$) is the gravitational acceleration; F_{sr} (s^{-1}) is the water exchange between roots and the soil.

This equation is used to describe soil water movement in both the unsaturated and saturated zones. The groundwater table (i.e., the interface between the unsaturated and saturated zones) is explicitly represented.

Water transport in roots along the vertical direction is described as follows:

$$\frac{\partial}{\partial z}\left[K_{ra}\frac{\partial(\psi_r - \rho_w g z)}{\partial z}\right] + F_{sr} = 0 \tag{2}$$

where K_{ra} ($m^2 \cdot s^{-1} \cdot Pa^{-1}$) is the axial hydraulic conductivity of roots per unit area; and ψ_r (Pa) is the root water potential. Meanings of the other symbols are the same as those in equation (1). Equation (2) is based

on the assumption that water transport in roots can be approximately represented by the Poiseuille law. Similar approaches are used by *Mendel et al*. [2002] and *Amenu and Kumar* [2008].

Water exchange between roots and soil is expressed by the equation below:

$$F_{sr} = K_{rr} S_r (\psi_s - \psi_r) \tag{3}$$

where K_{rr} ($m \cdot s^{-1} \cdot Pa^{-1}$) is the root radial hydraulic conductivity per unit of root surface area; S_r ($m^2 \cdot m^{-3}$) is the surface area of roots which absorb or release water per unit volume of soil; ψ_s (Pa) is the soil water potential; ψ_r (Pa) is the root water potential. This equation is based on the understanding that the water exchange between roots and the soil is primarily a passive process (i.e., the water flux is driven by the water potential difference between roots and the soil). This representation of root–soil water exchange is similar to that of *Landsberg and Fowkes* [1978]. Roots absorb water (i.e., the water exchange F_{sr} is positive) when the soil water potential is higher than the root water potential. On the other hand, roots release water (i.e., the water exchange F_{sr} is negative) when the root water potential exceeds the soil water potential. This unique phenomenon that water can flow from root to soil is the key component of the HR process.

Water movement in the soil (equation (1)) and water transport in roots (equation (2)) are linked through the root–soil water exchange represented by equation (3). These three equations are solved simultaneously to obtain the distribution of soil moisture and the water exchange between roots and the soil. In this way, the HR process and the water movement in both the unsaturated zone and the saturated zone are closely coupled.

Plant transpiration is calculated by uniting the method of electric analogy based on Ohm's law and the Penman-Monteith method. In the method of electric analogy [e.g., *Lhomme et al*., 2001], plant transpiration is estimated based on the soil water potential in the root zone, the water potential in leaves, and the hydraulic resistance in the soil and plant. Therefore, the effects of subsurface hydrologic processes on plant transpiration are represented. In addition, this approach facilitates a straightforward inclusion of the plant water storage and its impact on transpiration. In the Penman-Monteith method, the calculation of plant transpiration is not only driven by the direct use of the meteorological data but is also directly linked to the carbon assimilation through the stomatal conductance. The combination of the Penman-Monteith method and the method of Ohm's law analogy not only captures the plant transpiration affected by the meteorological conditions, photosynthesis process, and subsurface hydrologic processes, but also reduces the model's degrees of freedom by simultaneously having multiple constraints. For details on how the plant transpiration is computed in VIC+, the reader is referred to *Luo et al*. [2013].

In a similar manner, the carbon assimilation process involved in the plant transpiration is simultaneously represented through two coordinated perspectives using (1) a diffusion method, and (2) the modified Farquhar biochemical model. That is, the calculation of carbon assimilation is constrained as a consequence of the interplay of the stomatal and biochemical limitations simultaneously.

Representing the same process simultaneously from different perspectives is part of a modeling strategy introduced into the VIC+ model [*Luo et al*., 2013]. This is a new strategy in the land surface modeling application. Introducing such constraints from the physics of the processes reduces the number of model parameters to be calibrated when new processes are added. Therefore, in the VIC+ model, only one more model parameter is added to the VIC model's calibration list despite of the various new processes briefly described above being added to the VIC-3L model. Moreover, this new modeling strategy can facilitate identifying any inconsistency, should it exist, among different parameterizations.

In summary, the VIC+ model integrates HR, water movement in the unsaturated zone and unconfined aquifer, and plant transpiration with other land-surface water and energy processes of the VIC-3L model. The upper boundary condition of Richards equation (i.e., equation (1)) is determined by the land-surface water balance calculation. The flux boundary condition can be infiltration or soil evaporation. The calculation of plant transpiration produces the sap flux at the root collar, which is the upper boundary condition for the equation of root-water transport (i.e., equation (2)). Driven by these boundary conditions, equations (1)–(3) are solved to generate the updated distribution of soil moisture in the soil column. The updated soil moisture state is used in the calculations of soil evaporation, surface runoff, subsurface runoff, and plant transpiration at the next time step. Detailed descriptions of the methods for coupling these processes are provided in *Luo et al*. [2013]. The VIC+ model has been evaluated with analytical solutions and with

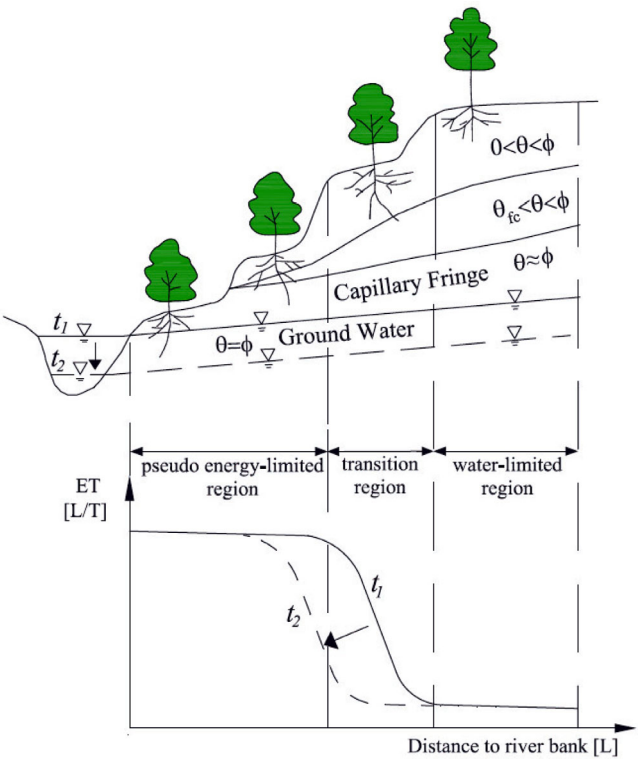

Figure 1. A schematic illustrating locations of the vegetation roots, subsurface soil water, and the GWTDs in relation to time and the three regions (i.e., pseudo energy-limited region, transition region, and water-limited region).

observations from two AmeriFlux sites: the "Duke Forest Loblolly Pine (US-Dk3)" site and the "Blodgett Forest (US-Blo)" site located in North Carolina and California of United States, respectively. Observed soil moisture, energy flux, and gross primary productivity at hourly or daily time scales are used in the validation process. The VIC+ model simulated results compare very well with analytical solutions and reasonably well with the observations, which provide credence for the present study.

3. Numerical Experiments

The VIC+ land surface model is used to conduct a series of numerical experiments to investigate the impacts on plant transpiration of the following factors: (1) GWTD, (2) HR, (3) vegetation type, (4) soil type, (5) precipitation conditions, and to a lesser extent (6) climate type. We designed the numerical experiments by visualizing conceptually that plants distribute spatially over hillslopes at a landscape scale, as shown in Figure 1, to capture the different scenarios that roots come into contact with groundwater. Specifically, the relationships between plant transpiration and GWT under a steady state condition are investigated in which the moisture state of soils surrounding roots depends on the location of the GWT. To capture the various scenarios, this study employs soil columns endowed with different maximum GWTDs. This is constructed as follows: we set up 10 basic soil columns for each scenario studied. Each soil column is 15 m deep, consists of a unique soil type, has a fixed root zone dictated by the vegetation type, and is assigned a maximum GWTD (i.e., a lower limit for GWT). The maximum GWTDs employed start from 1 m as the representative scenario next to the river, and with a 1 m increment, gradually increased to 10 m as the representative scenario at a location sufficiently far away from the river and uphill. The lowest of the maximum GWTD is set at 10 m because latent heat flux remains unchanged when the GWT approaches that depth as shown by *Maxwell and Kollet* [2008] and further affirmed by this study. The groundwater flow is considered in an implicit manner. Basically, the GWTD is first determined by the evapotranspiration, precipitation, and surface runoff, and the lateral subsurface flow is introduced afterward so that the prescribed maximum GWTD is maintained. For instance, if, under the forcing conditions of a climate, the GWT falls below the prescribed lower limit at the end of one time step, the unsaturated soil below the limit is restored to be saturated to keep the GWT at the specified lower limit. This has the same effect of having lateral flow recharging this soil column. The present study has included the feedback between transpiration and the GWT. In this study, each 15 m deep soil column is evenly discretized into 2 cm thick sublayers and its numerical experiment is carried out with an hourly time step for VIC+.

Constructing the numerical experiments in this manner makes it easier to track the interaction of the groundwater with the soil water and vegetation roots, and facilitates the exploration of the mechanisms involved in HR. To fully investigate the impacts of the interactions of GWTDs with HR, this study considers three vegetation types (coniferous tree, shrub, and grass), three soil types (clay, loam, and loamy sand), three different climate conditions (dry, moderate, and wet), and two scenarios (with and without HR). From the computational point of view, a full permutation of these parameter variations gives 54 different cases, and within each case, there are 10 soil columns to be studied and each column is solved until a steady state

is reached. However, since HR plays a more important role in drier climates, which is the focus of this study, only a subset of the 54 combinations was considered. We started first by investigating 18 cases which represent all possible combinations under the dry climate condition, i.e., 3×3×1×2 (three vegetation types by three soil types by one dry climate by HR and no-HR scenarios). Then we supplemented the study by considering the impact of precipitation conditions focusing only on coniferous tree as the vegetation and loam as the soil. A preliminary sensitivity study on the impact of climate type has also been introduced for the same setup with the coniferous tree as the vegetation and loam as the soil, but under dry climate.

In the following discussion, HR experiments refer to the experiments that HR is accounted for in running the VIC+ model, while the no-HR experiments have HR turned off. Thus, the difference is that in the no-HR cases, there is no root–soil water exchange even when the root water potential is higher than the soil water potential in equation (3).

For the three vegetation types, not only are the root depths different for each type but also are their root distributions. Assuming the root–soil water exchange occurs at live fine roots, the parameter S_r, referring to the surface-area density of live fine roots in equation (3), can be derived from the distribution of live fine roots and the total surface area of live fine roots per unit ground area (i.e., the live fine root area index; LFRAI). The distribution of live fine roots along the vertical direction is expressed by an asymptotic equation [*Gale and Grigal*, 1987; *Jackson et al*., 1997]:

$$Y = 1 - \beta^d \tag{4}$$

where Y is the cumulative root fraction from the ground surface to the depth d in centimeter; β is the extinction coefficient. Equation (4) represents the general circumstance that most roots grow in the shallow soil. In the numerical experiments, the maximum root depths are assumed to be 5, 4, and 2 m, respectively, for coniferous tree, shrub, and grass. The parameter values for the three vegetation types are given in Table A1. The physiology of the plants has not been considered in that the root parameters summarized in Table A1 remain the same regardless of time and climates.

Each soil column in the numerical experiments contains only one soil type. Soil parameters related to the three types, clay, loam, and loamy sand, in VIC+ include saturated hydraulic conductivity, porosity, residual soil water content, and the van Genuchten parameters to link the soil water potential to soil water content and soil hydraulic conductivity [*van Genuchten*, 1980]. These parameters are obtained from the database of the ROSETTA model maintained by the Agricultural Research Service of United States Department of Agriculture. Relevant soil parameters are described in the Appendix A and listed in Table A2.

For most numerical experiments, the meteorological forcing inputs (e.g., precipitation, air temperature, solar radiation, wind speed, and air pressure) are based on the observed data from year 2004 at the Blodgett Forest (US-Blo) site. The meteorological data are directly used except for precipitation which is scaled to get the dry, moderate, and wet precipitation conditions. Specifically, we first calculate the potential transpiration of coniferous trees by using the observed meteorological data of year 2004 from the Blodgett Forest (US-Blo) site assuming that the soil water supply does not constrain the transpiration. The annual amount of such potential transpiration is estimated to be 740 mm. Then the hourly precipitation time series for dry, moderate, and wet conditions are obtained by scaling the observed 2004 hourly precipitation time series so that the annual total precipitation amounts to 50%, 70%, or 100%, respectively, of the annual potential transpiration. These three precipitation conditions are denoted as P50 (dry), P70 (moderate), and P100 (wet), respectively. The 2004 precipitation amount for P100 is scaled to 740 mm to account for the situation that at the steady state, the maximum possible amount of the transpiration from VIC+ would be at its potential (740 mm) when there is no net surface and subsurface runoff and any other loss. Such an approach of generating the forcing input for conducting numerical experiments has been widely employed in other studies [e.g., *Walker and Houser*, 2004; *Maxwell and Kollet*, 2008; *Ferguson and Maxwell*, 2010]. The 1 year forcing inputs obtained in this way are repeated to drive the VIC+ model for the numerical experiments.

For all of the numerical experiments, the groundwater table is initiated at 0.5 m below the ground surface and the simulation carries on until it reaches a dynamic equilibrium state, namely the mean values of both plant transpiration and the groundwater table depth vary within the prescribed convergence limits. This steady state is achieved at an annual scale under which the pattern of the hourly time series for each variable repeats from year to year. When the precipitation amount is comparatively high, the GWTD becomes

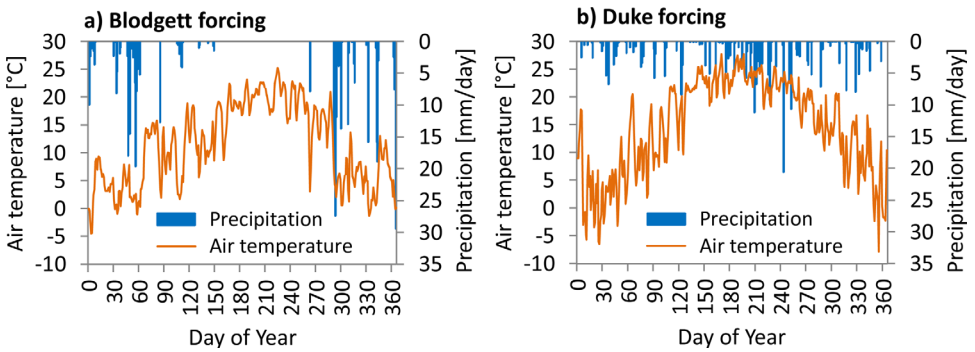

Figure 2. Forcing input of precipitation (P50 condition) and air temperature based on the forcing data of (a) Blodgett Forest (US-Blo) site in California and (b) Duke Forest Loblolly Pine (US-Dk3) site in North Carolina.

stable and the steady state is achieved after a few years of the simulations. In many cases, mostly those involving shrubs and grasses, the transpiration and GWT reach steady states at a GWTD shallower than its preset lower limit, computation is not carried out for deeper GWTDs for the soil columns under those sets of simulation parameters.

The precipitation pattern of the Blodgett site has the Mediterranean climate in which the precipitation mainly occurs from October to May with very few rainfall events from June to September. Also used, but only in a preliminary sense for sensitivity comparison, is the precipitation pattern from the Duke Forest (US-Dk3) site, which has the oceanic climate. Its precipitation is more evenly distributed year round. Figure 2 shows the P50 precipitation condition and the air temperature based on data from the Blodgett and Duke sites, respectively. The inputs of P50 from the Duke site are generated in the same way as those from the Blodgett site.

In the follow discussions, transpiration, GWTD, and flow quantities are all expressed in terms of annual means unless otherwise noted.

4. Results and Discussions

4.1. Transpiration–Groundwater Depth Relationship

The relationship between transpiration and mean groundwater table depths (abbreviated to "transpiration–GWTD relationship") from the steady states are presented in this section. Figure 3 summarizes the transpiration–GWTD relationships from 18 experiments. It can be seen that, under the dry climatic condition, HR can significantly promote the tree transpiration (Figure 3, first row) by an average of 14.5% (loam), 13.6% (loamy sand), or 23.0% (clay) relative to no-HR, when the GWTD is in the 3–6 m range. Also, the effects of HR vary with the GWTD. For the shrub cases (Figure 3, second row), the impact of HR on transpiration is less significant, ranging in average from 9% to 13% when the GWTD lies between 3 and 5 m. For the grass cases (Figure 3, third row), the HR impacts are mostly less than 7%.

The effect of HR on transpiration is not evident when the GWT is only 1 or 2 m below the surface for most cases (see Figure 3 except for Figure 3c). This is because a fraction of tree roots is in constant contact with groundwater: 11% of the tree roots locates between 1 and 2 m below the ground, while 2% below 2 m from the surface. The root zone is further divided into shallow and deep root zones: the former is from the depth of 0 to 1 m, and the latter is from 1 m to the maximum root depth (i.e., 5, 4, and 2 m for the tree, shrub, and grass types, respectively). Roots in the shallow zones have access to abundant soil water to sustain its transpiration when the GWT is close to the surface. The influence of HR is, thus, minimal and the transpiration is primarily determined by atmospheric conditions (i.e., energy limited).

An examination of Figure 3a (grey line) further shows that the HR contribution to transpiration increases as the GWT drops from 1 m and reaches a maximum value of 80.7 mm/yr when the GWT is 6 m deep. As the GWT descends, soil moisture in the shallow root zone decreases and that raises constraint on soil water for transpiration demand. However, the deep root zone is still comparatively wet as long as GWT remains not far below the root zone such that HR could transfer soil water from the wetter deep root zone to the drier

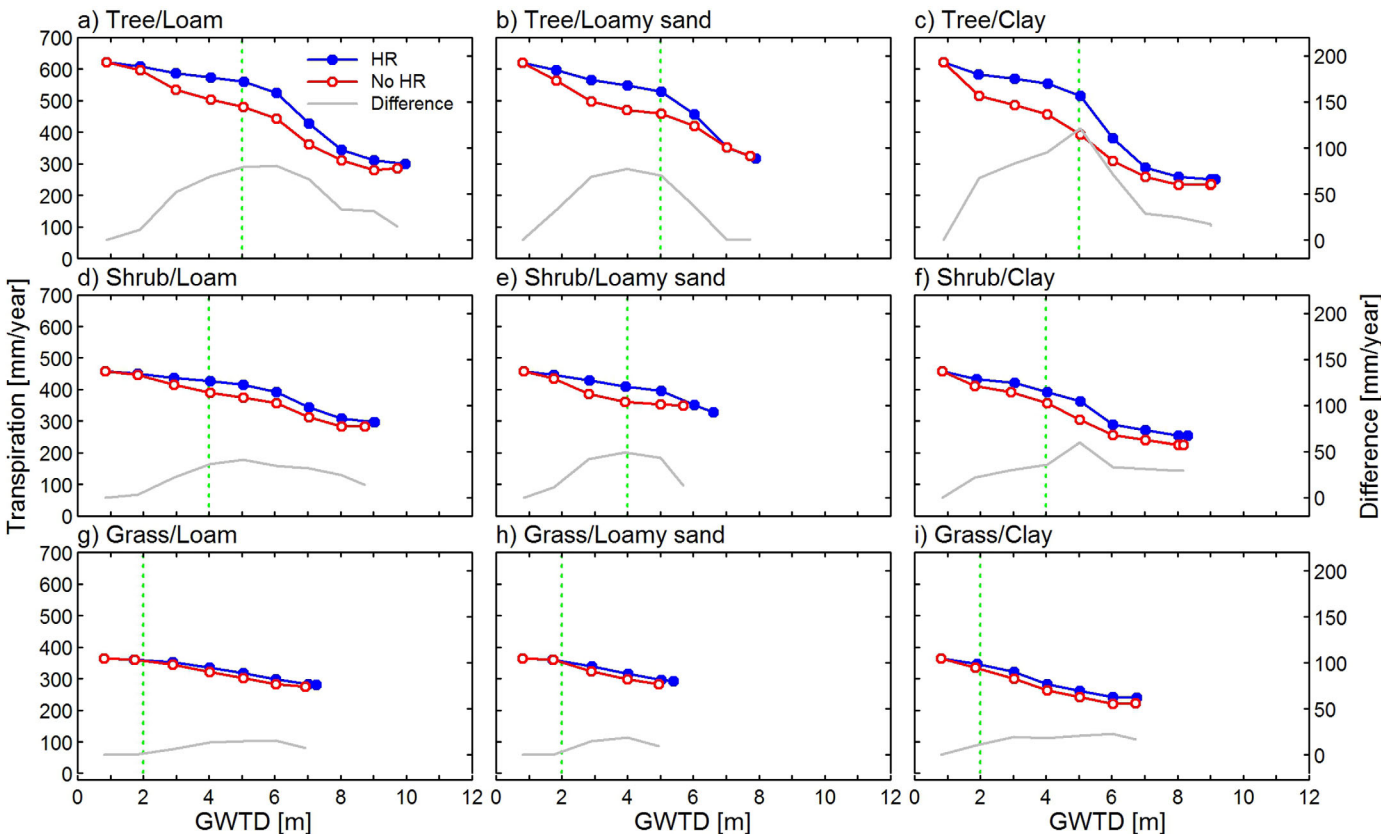

Figure 3. Comparisons of transpiration–GWTD relationships between HR and no-HR experiments for three vegetation types ((first row) Coniferous tree, (second row) Shrub, and (third row) Grass) and three soil types ((left column) Loam, (middle column) Loamy sand, and (right column) Clay) under the precipitation condition of P50. The differences are plotted by using a secondary *y* axis. The dashed green lines indicate the root zone depths (i.e., 5, 4, and 2 m for coniferous tree, shrub, and grass, respectively).

shallow soil layer. This promotes plant transpiration through water uptake by shallow roots even though 87% of the roots are within the 1 m soil layer below the land surface.

The effect of HR on transpiration then starts to decrease from its maximum when the GWT continues to descend below the depth of 6 m (see Figure 3a). As the GWT drops farther away from the root zone, soil in the deep root zone becomes drier. Thus, the effect of upward HR process on transpiration gradually diminishes due to the scarcity of the available soil water resources. The transpiration is therefore controlled by the precipitation, and the differences in transpiration between HR and no-HR approaches become very small.

The results as discussed clearly show that the HR effects on transpiration are determined by the available soil moisture to the roots and that is how groundwater makes its impact. The mechanism of HR can be explained from the soil moisture state of the root zone by examining how it plays a role on the transpiration on one hand, and how it is being affected by the location of the GWT on the other. From the transpiration perspective, we can relate three regions of the transpiration–GWTD curve each to its corresponding dominant mechanism. Using Figure 3a as an example, the initial mildly sloped segment of the curve represents a pseudo energy-limited region since transpiration is at or close to a rate controlled by the available energy. Whereas, the flatter segment at the bottom of the curve represents a water-limited region as transpiration there is controlled by available water. The sharp sloped segment in the middle of the curve is a transitional region between the two transpiration modes. Corresponding to these three transpiration regions are three ranges of GWTD. They can be denoted as shallow, intermediate, and deep, respectively. GWT within each GWTD range results in a different moisture state in the root zone. Three soil moisture states, rich, moderate, and poor, are invoked when GWT goes from shallow, intermediate to deep, respectively. The range of GWTD, the soil moisture state of the root zone, and the transpiration mode are but different views on the same phenomenon. The GWTD relates to the cause, the soil moisture the effect, and the transpiration the

consequence. These terms are thus interchangeable. For instance, when the GWTD is within the shallow range, the root zone soil moisture state is rich, and the transpiration is pseudo energy-limited. Depending upon the distance to the river bank and water levels in the river, e.g., the water levels corresponding to t_1 and t_2 in Figure 1, position of the GWT within a soil column may change. As GWT fluctuates, the root zone soil moisture state for each column changes, and so does the transpiration. In the discussion that follows, these three views are taken together to explain the HR impacts.

It is important to point out that when HR is not included, the transpiration–GWTD relationship of the tree experiments (e.g., Figures 3a–3c) also exhibit the aforementioned three regions. This is consistent with the findings of the previous studies in which HR is not considered [e.g., *Maxwell and Kollet*, 2008; *Kollet and Maxwell*, 2008] and where the three regions were defined as temperature controlled, groundwater controlled (transition), and precipitation controlled, respectively. However, without including HR, the pseudo energy-limited region is significantly reduced while the transitional region is largely increased. The water-limited region remains very much the same. Specifically, Figure 3a shows that the pseudo energy-limited region for the no-HR case is from surface to 3 m depth (corresponding to the transpiration value between 621 and 586 mm/yr), which is a 3 m reduction from the HR case. On the other hand, the transitional region for the no-HR case is from 3 to 9 m—a 3 m increase.

HR extends the GWTD range of the rich soil moisture state in the root zone because when the GWT is within or close to the bottom of the root zone, soil water can be pumped upward through HR to provide water for transpiration. If certain conditions are met, the pumped upward soil water could be enough to sustain the transpiration at a rate close to the value controlled by the available energy. With this pseudo energy-limited region extended by HR, the transitional region is shrunk. On the other hand, for the no-HR case, this pseudo energy-limited region can only be sustained with shallower GWT, e.g., at a depth of about 3 m below the surface (see Figure 3a). This is why the shallow GWTD range is thinner and that leaves a thicker transitional region. The water-limited region remains about the same with and without HR since the GWT is too far away from the bottom of the root zone to make a difference.

The different ways HR impacts on transpiration depend on which GWTD range that the GWT lies. This clearly demonstrates the critical roles plant roots can play in transpiration under a dry climate. It also supports our hypothesis that plants can modulate available soil moisture at the beginning stage of a dry period through HR, since the GWT at that stage has not yet dropped far below the bottom of the root zone (e.g., still within or about 1 m depth below the root zone in Figure 3a). In this case, the roots can tap soil moisture from the groundwater through HR to maintain a high transpiration rate for a period of time. For the case shown in Figure 3a, this period of time is the time that takes to drop GWT from 3 to 6 m on the blue curve. Once that happens, transpiration starts a transition to go from its initially high rate to a low rate, as the GWT continues to descend due to the dry condition. Toward the end of this stage, the plants and surface processes become decoupled from the subsurface processes. When the GWT further descends, the impact of the dry condition intensifies as plant roots have difficulties accessing groundwater to sustain the transpiration needs. The transpiration is reduced to a very small level and is controlled by precipitation (water limited). Without considering HR, the ability of plants with deep roots to sustain a dry period could be significantly underestimated. In other words, without the inclusion of HR, reduction in the transpiration could start much earlier as is shown by the red lines comparing to the blue lines in Figures 3a–3c, which could lead to different transpiration cycles as well as different water and energy cycles.

The shape of the transpiration–GWTD relationship curves is found insensitive to soil types for both the HR and no-HR cases as demonstrated in Figures 3a–3c, Figures 3d–3f, and Figures 3g–3i. *Soylu et al*. [2011] also obtained similar evapotranspiration–GWTD relationship curves for a few soil types in their model sensitivity experiments without including HR. A closer look shows that the HR-caused transpiration increments are different at the same GWTD for the three soil types. For loam, loamy sand, and clay, the maximum differences between HR and no-HR are, respectively, 80.7, 77.6, and 121.5 mm/yr, corresponding to GWTDs at 6, 4, and 5 m. These differences are mainly caused by the soil hydraulic properties which affect the distribution of moisture in the soil. This result is consistent with the finding of *Ryel et al*. [2002] that the increase of transpiration due to HR can be affected by soil characteristics.

Vegetation types affect the shapes of transpiration–GWTD relationship curves. The curves for the shrub and grass (Figures 3d–3i) are quite different from that for the tree (Figures 3a–3c). But, the differences between

HR and no-HR are smaller (with an averaged difference of 8% for shrub and 4% for grass) than those for the tree cases (with an averaged difference of 11%). These differences in the HR contribution are primarily caused by the dissimilar transpiration capacities associated with the different vegetation types. At the same GWTD, the shallow soil layer in the shrub experiments is wetter because shrubs have lower transpiration capacity compared to trees, which results in a lesser need of soil water. This thus results in a weaker upward HR process in the shrub experiments. For the same reason, the effect of HR on transpiration is further lessened as shown on transpiration in the grass experiments under this dry precipitation condition (i.e., P50). These results of the less sensitivity of transpiration to soil types than to vegetation types are consistent with those of *Condon et al.* [2013] in which HR was not considered. From the 18 experiments shown in Figure 3, we can clearly observe the different impacts of HR on transpiration over the three GWTD ranges for each soil and vegetation type. By employing soil columns, this study is able to use fixed settings and explores underlying mechanism and dynamics through various parameter combinations. As for a watershed-based approach, however, it may be difficult to assemble such combinations under desired conditions. In addition, a watershed-based approach may lead to noisy transpiration–GWTD relationship curves, as shown in *Condon et al.* [2013], due to potential equifinality effects, which could make it harder in identifying the causes and underlying dynamics. The watershed-based study is valuable for it provides a general picture of the studied watershed with more possible scenarios. In a way, the present column study complements it by zooming in to look into the mechanism.

The mechanism of HR process can be clarified further by examining the hydraulic distributed water, upward diffusion of soil water, and the daytime uptake by roots. They are investigated in sections below.

4.2. Hydraulically Redistributed Water

Hydraulically redistributed water (HRW) refers to the amount of water flowing from roots to soil and can be used to identify the intensity of HR. Soil water can move from the deep root zone to the shallow root zone through the upward HR process, which usually occurs at nighttime in dry conditions, or from shallow root zone to deep root zone via the downward HR process, which usually occurs after rainfall events. The intensity of the upward HR process can be revealed by the HRW amount in the shallow root zone (abbreviated to shallow HRW) and the intensity of the downward HR process by the HRW amount in the deep root zone (abbreviated to deep HRW). Results shown in Figure 4 apply only to the dry periods for the shallow HRW and to the time periods after rainfall events for the deep HRW. Both the shallow and deep HRWs are analyzed in this section to shed light on the role of HR in the surface water–groundwater interactions.

Figure 4 shows the HRW–GWTD relationships under the dry precipitation condition of P50. Figure 4a shows that the shallow HRW is close to zero when the GWT is around the 1 m depth. This is because the shallow root zone is wet when the GWT is shallow even after the daytime transpiration. Thus, the water-potential gradient between the deep root zone and the shallow root zone at night is mild, which does not cause any evident upward HR. When the GWT falls down but still within the root zone, the shallow HRW rises and reaches its maximum with the GWT around the root zone bottom (5 m). This is because under the dry climatic condition, the shallow root zone becomes dry after the daytime transpiration, while the deep root zone is wet due to the presence of the GWT. Thus, the water-potential gradient between the shallow and deep root zones becomes large, which boosts the upward HR. When the GWT continues to descend from the root zone bottom to 1 m below, the shallow HRW is still high (close to its maximum) due to the soil water diffusion process which brings soil water from the GWT at the 6 m depth to the bottom area of the root zone. As such, the water-potential gradient is kept high and thus, the shallow HRW remains high. However, when the GWT descends further, the soil water diffusion process is not strong enough to keep the root zone bottom wet, thus, the water-potential gradient between the deep and shallow zones becomes milder. The shallow HRW decreases due to the attenuation of the upward HR process. Figure 4a also shows that the shallow HRW levels off as the GWT is more than 4 m below the root zone bottom as the effect of groundwater on the root zone's wetness diminishes. Under such a situation, the presence of wet soil around the deep roots is due mainly to the infiltration, percolation, and downward HR of the rainfall water to the deeper soil layers. In summary, the upward HR enhances the plant transpiration. This explains why the shapes of the shallow HRWs shown in Figure 4 are similar to the shapes of the grey lines shown in Figure 3 which represent the difference between HR and no-HR experiments.

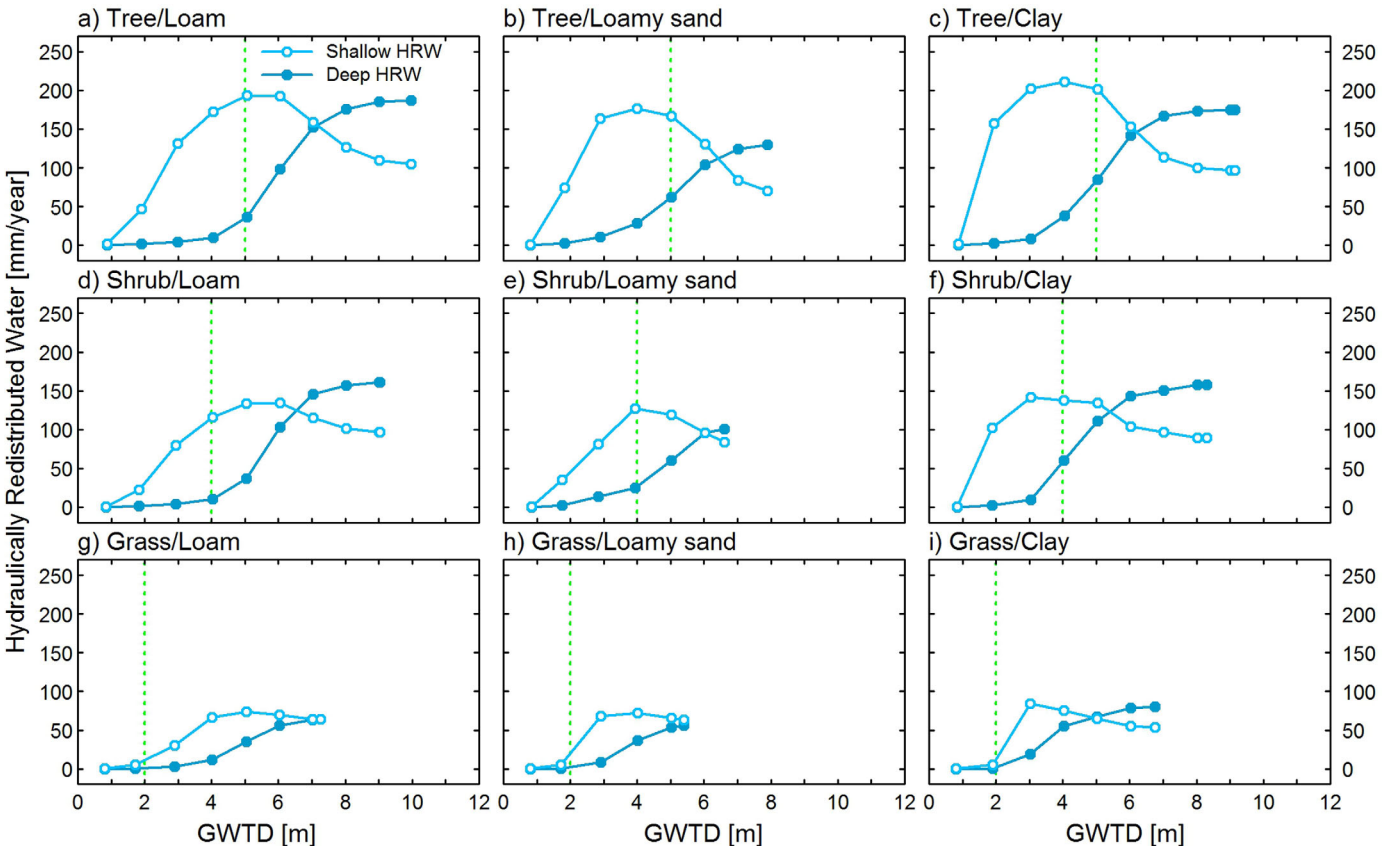

Figure 4. Shallow HRW–GWTD relationships and Deep HRW–GWTD relationships for three vegetation types ((first row) Coniferous tree, (second row) Shrub, and (third row) Grass) and three soil types ((left column) Loam, (middle column) Loamy sand, and (right column) Clay) under the precipitation condition of P50. Shallow HRW and deep HRW refer to the amount of hydraulically redistributed water in the shallow root zone and the deep root zone, respectively. The shallow root zone spans from the ground to the 1 m depth, and the deep root zone spans from the 1 m depth to the root zone bottom. The dashed green lines indicate the root zone depths (i.e., 5, 4, and 2 m for coniferous tree, shrub, and grass, respectively).

With respect to the deep HRW, Figure 4a shows that it is very low when the GWTD is smaller than about 4 m. This is because both the shallow and deep root zones are wet and the water-potential gradient from the shallow root to the deep root zones is gentle. However, the deep HRW starts to increase when the GWT drops below 4 m. Under this situation, the deep root zone starts to become dry and it gets drier as the GWT further descends. This increases the water-potential gradient from the shallow root zone to the deep root zone after the rainfall events and hence promotes the downward HR process. Figure 4a also shows that the deep HRW levels off after it reaches its maximum value which has a similar total amount as the maximum shallow HRW. This is expected if the total time period for the downward HR process is similar to that for the upward HR process because the maximum values of the water-potential gradients would be similar for both ways. The influence of groundwater on root zone soil moisture through the downward HR process also becomes minimal when the GWT is far from the root zone. This again reflects that the interaction between the GWT and the surface processes is decoupled at that depth.

Impacts of soil types can be observed from a comparison among Figures 4a, 4b, and 4c which shows that, for both the shallow HRW and deep HRW, the HRW–GWTD relationship curves of the experiments have, respectively, similar shapes. The differences among them are mainly due to the different soil hydraulic properties which affect the movement and distribution of the soil water. This result agrees with *Ryel et al.* [2002] on that the HRW amount is affected by soil hydraulic properties.

As for the differences in HRW among vegetation types, Figure 4 demonstrates that, for both the shallow HRW and deep HRW, the shapes of the HRW–GWTD relationship curves for the shrub and grass experiments are similar in trend to those of the tree experiments although the amounts differ. The shallow HRW amounts of the shrub experiments are lower than those of the corresponding tree experiments. The reason is that the shrub has a transpiration capacity lower than that of the tree, which leads to a wetter shallow soil

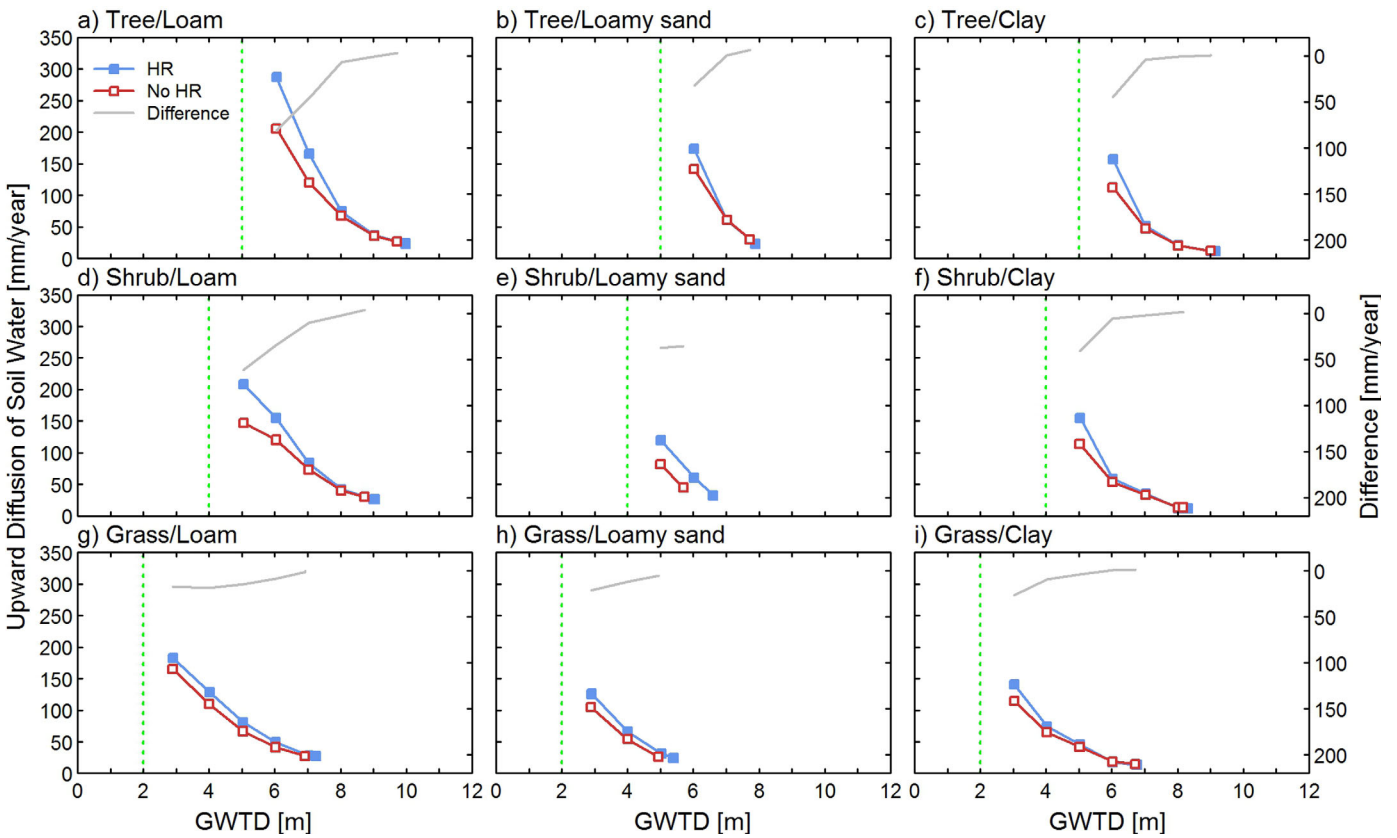

Figure 5. Comparisons of upward diffusion–GWTD relationships between HR and no-HR experiments for three vegetation types ((first row) Coniferous tree, (second row) Shrub, and (third row) Grass) and three soil types ((left column) Loam, (middle column) Loamy sand, and (right column) Clay) under the precipitation condition of P50. The amount of upward soil water diffusion (abbreviated to upward diffusion), through a horizontal cross-section which is located 0.5 m below the root zone bottom, is calculated. The dashed green lines indicate the root zone depths (i.e., 5, 4, and 2 m for coniferous tree, shrub, and grass, respectively). The differences between HR and no-HR experiments are plotted by using a secondary *y* axis (note: the ordinates for the differences are reversed for clarity).

layer, and thus a weaker upward HR process. For the same reason, the grass experiments show even smaller amounts of the shallow HRW. For the deep HRW, the lower transpiration capacity of the shrub results in a wetter deep root zones. Thus, they give smaller amounts of the deep HRWs than the corresponding tree experiments for all three soil types (Figure 4). Similarly, the deep HRW amounts for the grass experiments are lower than those of the corresponding shrub experiments regardless of soil type.

4.3. Upward Diffusion of Soil Water

Under dry climatic conditions, soil water can move upward from the groundwater table to the comparatively drier shallow soil through the diffusion process [e.g., *Soylu et al.*, 2011]. The amount of the upward diffusion depends on the position of the GWT. To investigate the utilization of groundwater by plants when the GWT is below the root zone bottom and the effectiveness of the upward HR in assisting the utilization of such soil water, we calculate the amount of upward soil water diffusion (abbreviated to upward diffusion) through a cross-section located 0.5 m below the root zone bottom.

Figure 5 compares the upward diffusion–GWTD relationship curves of HR experiments with those of no-HR experiments under the precipitation condition of P50. It can be seen that, for both experiments, the upward diffusion is evident when the GWT is within the distance that can be reached by diffusion below the root zone bottom, and it declines abruptly as the GWT falls down below that. The upward diffusion becomes minimal when the GWT falls 2–4 m from the root zone bottom, indicating that at some point the link between groundwater and the shallow surface processes becomes weak. That is, the groundwater is decoupled from the surface processes. Figure 5 shows that HR enhances the upward diffusion, comparing to the no-HR case, when the GWT is below but close to the root zone bottom. With further lowering of the GWT, the enhancement on the upward diffusion by HR is reduced and the difference between HR and no-

HR eventually disappears. The enhancement in the upward diffused soil water comes about because the soil moisture in the deep root zone with HR becomes drier than that with no-HR. As such, there is a larger water-potential gradient within the region up to some distance, e.g., about 0.5 m, below the root zone bottom for HR experiments. As the GWT falls further away from the root zone, the soil moisture difference caused by HR and no-HR around this affected region decreases and eventually becomes negligible. For example, Figure 5a shows that HR promotes the upward diffusion by 81 mm (from 206 to 287 mm) when the GWT is 1 m below the root zone bottom (i.e., at the 6 m depth), but the HR contribution to the upward diffusion amount is only 6 mm (from 68 to 74 mm) when the GWT is deeper at 3 m below the root zone bottom (i.e., at the 8 m depth). In summary, results from Figures 3–5 show that the effects of the combined diffusion and HR processes not only result in the largest differences between HR and no-HR experiments to occur around the root zone bottom, but they also make the utilization of the groundwater resource below the root zone bottom possible. Furthermore, results in Figures 3 and 5 with HR demonstrate that not only the GWT dynamics and diffusion process affect the transpiration, but also the HR and transpiration processes (surface processes) affect the diffusion process (a subsurface process), in which HR (both the upward HR and downward HR) serves as one important linkage in facilitating their interactions.

The amount of the upward diffused water is influenced by the soil properties associated with the soil types for both the HR and no-HR experiments as illustrated in Figure 5. The soil properties affect not only the soil wetness of the root zone but also the soil water distribution below the root zone. Therefore, the soil water-potential gradients around the aforementioned roughly 0.5 m range are different for the different soil types, leading to the different amount in the upward diffusion. For example, when the GWT is at the 6 m depth (Figures 5a–5c), the upward diffusion amounts for loam, loamy sand, and clay are, respectively, 287, 173, and 157 mm with HR; and are, respectively, 206 (i.e., 81 mm less), 141 (i.e., 32 mm less), and 112 mm (i.e., 45 mm less) with no-HR.

In contrast to the small influence on the transpiration (Figure 3) and HRW (Figure 4) by the soil types, the influence on the upward diffusion by the soil types is more significant than that by the vegetation types (see Figure 5). This is because the upward diffusion process is a physically dominated process in which the soil properties play a primary role, while both the transpiration and the HRW processes are jointly affected by the physiology and physical principles in which vegetation properties, such as transpiration capacity and root distribution, play a larger role. These vegetation properties affect the soil moisture in the root zone and the water potential right below it. Figure 5 illustrates this point as it shows that the magnitudes of the upward diffusion amount are different. For instance, when HR is considered and when the GWT is at 1 m below the root zone bottom with the loam soil (i.e., Figures 5a, 5d, and 5g), the amounts of the upward diffusion with HR are 287, 209, and 183 mm, respectively, for tree, shrub, and grass.

4.4. Daytime Uptake by Roots

Daytime uptake by roots supplies water for transpiration as HR usually is not evident in daytime. The daytime uptake by roots is represented by both shallow and deep root zones defined in section 4.1.

Conceptually, differences in daytime root uptake between the HR and no-HR experiments are due mainly to the difference in the available soil water. This available soil water for root uptake includes water distributed from both upward HR and upward diffusion processes, but the upward HR process plays a dominate role as the diffusion is a slow process. Thus, the differences in uptake with HR and no-HR experiments are mainly contributed by the upward HR process. This can readily be seen by comparing the grey lines, which representing the differences between HR and no-HR experiments, in Figure 6, first row, with the light blue lines representing the shallow HRW in Figure 4, first row. The shapes and magnitudes between these two sets of lines are quite similar and that affirms the dominant role HR plays in resulting in the large uptake differences. Furthermore, these lines are also similar to the corresponding grey lines in Figure 3, first row, demonstrating that the main differences in transpiration between HR and no-HR experiments are dominated by the differences contributed by the shallow HRW. Since the total shallow uptake includes both transpiration and the amount due to the downward HR, the grey curves in Figure 3, first row, have smaller magnitudes.

The shapes of the daytime root uptake–GWTD relationship curves for trees in the shallow root zone for different soil types, as shown in Figure 6, first row, are similar among those with HR, and are also similar

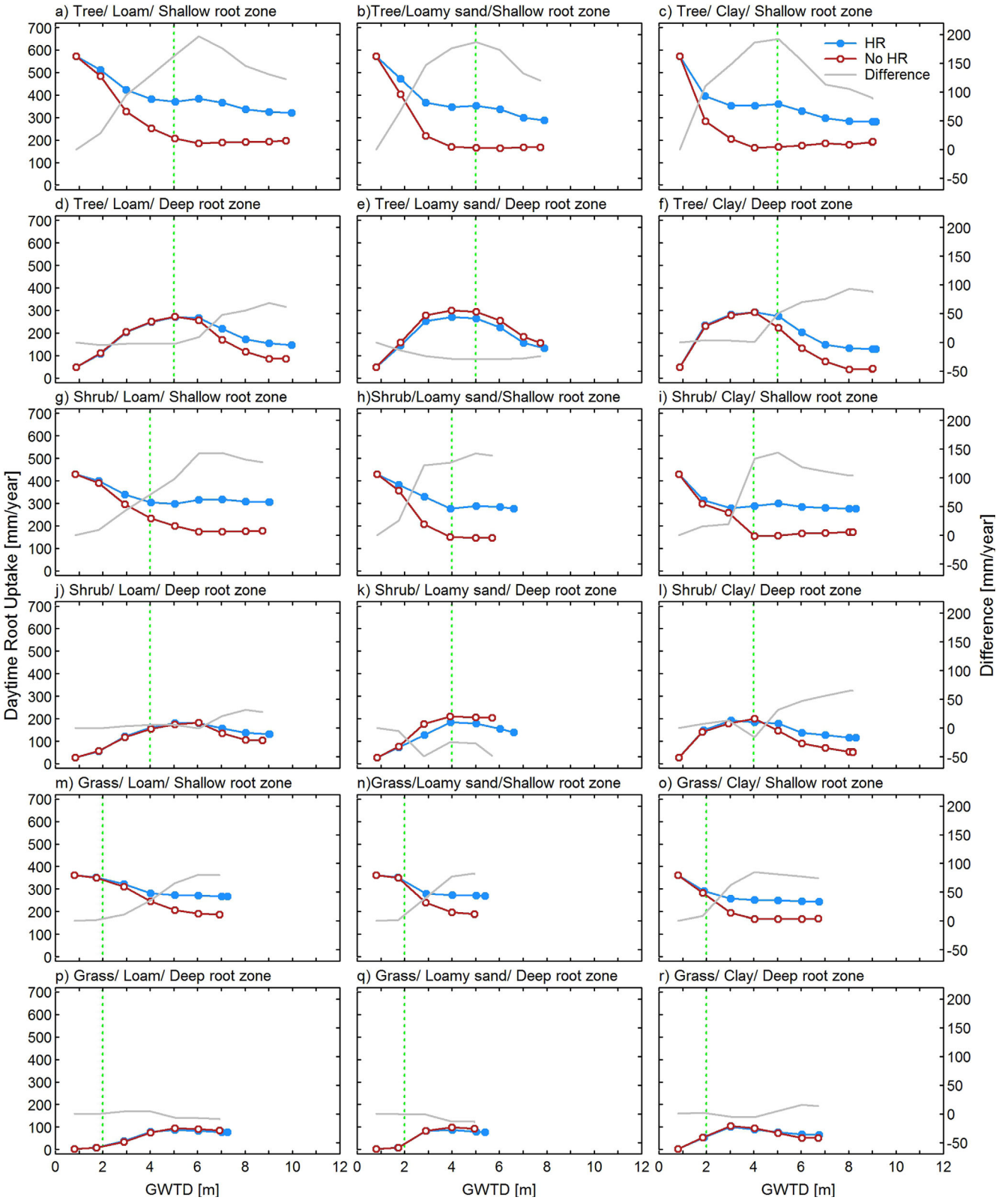

Figure 6. Comparisons of daytime root uptake–GWTD relationships between HR and no-HR experiments for: (1) three vegetation types ((first and second rows) Coniferous tree, (third and fourth rows) Shrub, and (fifth and sixth rows) Grass); (2) two parts of the root zone ((first, third, and fifth rows) Shallow root zone and (second, fourth, and sixth rows) Deep root zones); and (3) three soil types ((left column) Loam, (middle column) Loamy sand, and (right column) Clay). The differences between HR and no-HR experiments are plotted by using a secondary *y* axis. The precipitation condition is P50. The dashed green lines indicate the root zone depths (i.e., 5, 4, and 2 m for coniferous tree, shrub, and grass, respectively).

among those with no-HR. Although trends are different, such similarities among HR and among no-HR cases are also observed across soil types for the deep root zone (i.e., Figure 6, second row). In terms of the patterns of these relationships, it can be clearly observed that as the GWT drops within the root zone, the daytime root uptake in the shallow root zone decreases since the shallow root zone becomes drier than the deep root zone, but in the meantime, the deep root zone increases its uptake accordingly. As the GWT drops below the root zone bottom, groundwater no longer effectively replenishes the deep root zone and thus its uptake decreases. As the GWT drops even further, root uptake of both the shallow and deep root zones tends to level off since plant transpiration is then primarily sustained by precipitation and the uptake process is almost decoupled from the groundwater. In addition, the shallow roots can be seen responsible for the major daytime uptake, as the shallow soil layer is where the major root mass concentrates.

This study also finds that the shallow roots and deep roots absorb water differently. When the GWT lies within the shallow root zone, Figure 6 shows that the daytime root uptake with HR is higher than that with no-HR. But when the GWT is deeper than 1 m, and the largest difference occurs in the vicinity of the GWT that maximizes the upward HRW as shown in Figure 4. The reason is that HR transfers soil water from the deep soil to the shallow soil layer during the nighttime, which then enhances the root uptake in the following day. This is one major way HR promotes transpiration.

When the GWT stays within the deep root zone, Figure 6 shows that the deep root zone daytime root uptake of HR is comparable with that of no-HR cases. But when the GWT drops below the root zone, the daytime uptake by deep roots with HR becomes higher for the loam and clay types, namely, the daytime uptake by deep roots is promoted by HR. The reason is that, at nighttime, HR pumps water from the deep root zone to the shallow root zone and it also creates a larger water-potential gradient below the deep root zone bottom, which enhances upward soil water diffusion to the deep root zone from the groundwater. For the loamy sand type, the shape of the deep root zone uptake with no-HR is similar to that with HR, but the magnitudes with no-HR are slightly larger. This is likely because soil water in the loamy sand is easier to be pumped up compared with other soils by the upward HR, such action makes the deeper soil layer drier. Thus, it leads to less uptake from the deep root zone with HR than that with no-HR. Similar daytime root uptake behaviors for both the shallow and deep root zones are observed for shrubs and grasses and for loamy sands and clays (Figures 6g–6r).

The preceding discussions explain how the shallow and deep root zones provide water to plant transpiration in the daytime. It is clear that HR is a crucial mechanism for this important phenomenon.

4.5. Effects of Precipitation Conditions

Under the moderate and wet precipitation conditions (i.e., P70 and P100), the shallow soil layer in the shrub and grass experiments becomes even wetter, which results in smaller effects of HR on the transpiration. This is why experiments on precipitation impact are only carried out for trees in loams. The transpiration–GWTD relationship curves are not sensitive to the soil types as shown in Figure 3. Loams are selected partly because the soil properties of loams lie between those of loamy sands and clays.

Figure 7a, a duplicate of Figure 3a, is repeated for the convenience of comparison among the three precipitation conditions. Similar to P50, the effect of HR on transpiration is evident for P70 and P100 for a wide range of the GWTDs, and the HR contribution to transpiration depends on the location of the GWTDs. For the HR included experiments, the transpiration–GWTD relationship curve under the P70 condition has the characteristics similar to that of the curve of the P50 condition, i.e., having three distinctive transpiration regions. However, under P100, the division among the three regions is blurred. That is, the transpiration does not change significantly over the three different GWTD ranges, indicating a lesser role the groundwater plays than that under the drier conditions. This is because under this wet precipitation condition, there is sufficient precipitation to keep the root zone soil moisture in the rich state. Since the transpiration is not supported by the groundwater, the transpiration decreases mildly as the GWT drops. For the no-HR experiments, the three regions can be observed for P70 and P50, but not so for P100.

As demonstrated in Figure 7, the transpiration–GWTD relationships are affected by precipitation. It can be observed that the transitional region in the transpiration–GWTD relationships diminishes as precipitation increases. However, impacts by HR stay about the same. The contribution of HR can again be understood

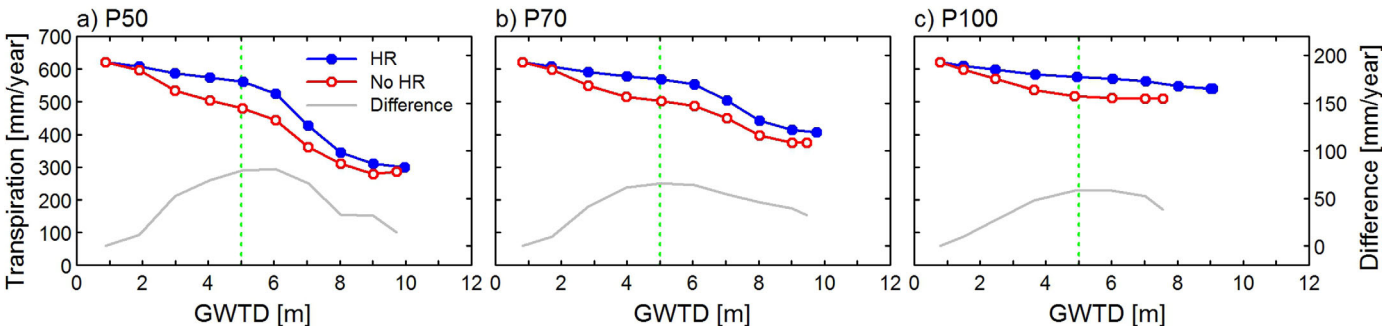

Figure 7. Comparisons of transpiration–GWTD relationships between HR and no-HR experiments under three precipitation conditions: (a) P50, (b) P70, and (c) P100. The vegetation type is coniferous tree and the soil type is loam. The differences are plotted by using a secondary *y* axis. The dashed green line indicates the root zone depth (i.e., 5 m).

by examining the interaction of shallow and deep HRWs, upward diffused water, and the daytime root uptake which are summarized in Figures 8–10, respectively.

For HRW, as summarized in Figure 8, it can be observed that with the increase of precipitation, more soil water becomes available for plant transpiration and thus the amount of shallow HRW reduces. The shape of the shallow HRW under P50 is similar to that under P70, but that is not the case under P100. The most noticeable difference is that the shallow HRW under P100 stays flat, rather than drops, after GWT is lowered below 6 m. This is because, under the wet precipitation condition, there is enough soil water available for plant transpiration. Thus, the transpiration is controlled mainly by the available precipitation. In this case, impact of the GWTD on the shallow HRW is limited. In other words, when the GWT is more than 6 m deep, the source of the HRW (e.g., around 150 mm/yr) originates from precipitation, not groundwater. That is, precipitation infiltrates and percolates to the 1–5 m depth range. Subsequently, soil moisture within the 1–5 m layer is redistributed to the soil layer of the 0–1 m depth.

As for the deep root zones, the amount of the deep HRW increases as precipitation increases from P50 to P70. This is because more water infiltrates into the shallow root zone, and is then redistributed by roots to the deep root zone. However, when precipitation increases from P70 to P100 and when the GWTD is greater than 5 m, the deep HRW amount decreases compared to those for P70 and P50. The reason is likely that the deep root zone becomes even wetter for P70 and P100, causing a reduction in soil water potential difference between the deep and shallow root zones, which damps the downward HR.

Figure 9 summarizes the upward diffused soil water under the three precipitation conditions with HR. It shows that the amount of the upward diffused soil water increases as precipitation decreases due to the increased gradient of soil water potential as discussed in section 4.3.

As for the daytime root uptake with HR, the higher the precipitation, the greater is the daytime root uptake in the shallow root zone as illustrated in Figures 10a–10c. It is higher for wetter conditions when GWT is

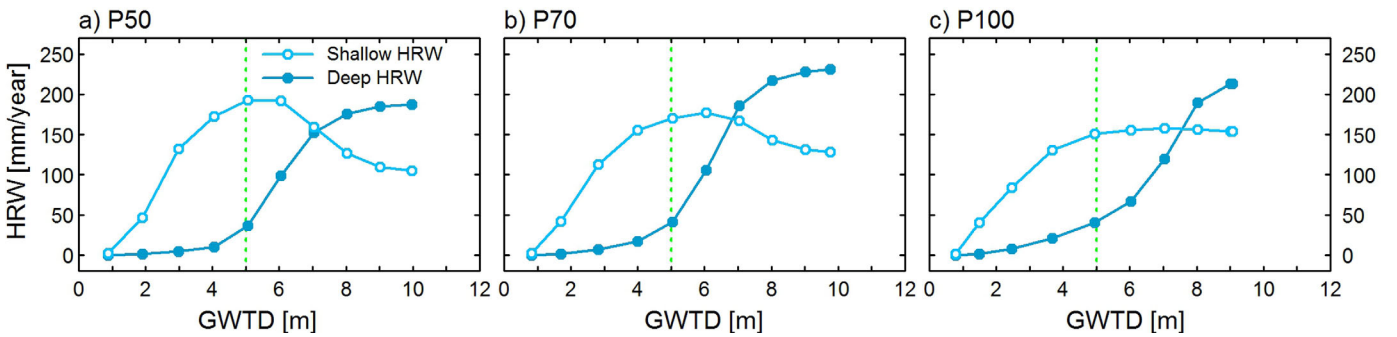

Figure 8. Shallow HRW–GWTD relationships and Deep HRW–GWTD relationships under three precipitation conditions: (a) P50, (b) P70, and (c) P100. The vegetation type is coniferous tree and the soil type is loam. Shallow HRW and deep HRW refer to the amount of hydraulically redistributed water in the shallow root zone and the deep root zone, respectively. The shallow root zone spans from the ground to the 1 m depth and the deep root zone spans from the 1 m depth to the root zone bottom. The dashed green line indicates the root zone depth (i.e., 5 m).

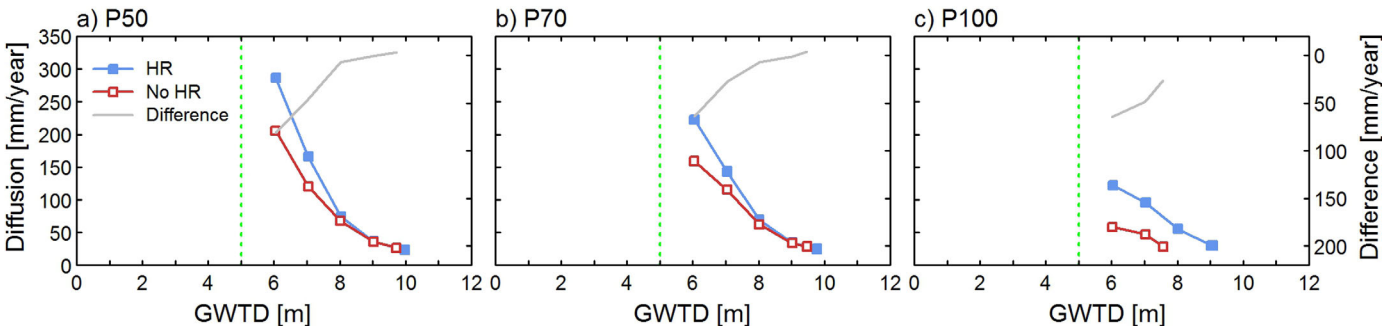

Figure 9. Comparisons of upward diffusion–GWTD relationships between HR and no-HR experiments for three precipitation conditions: (a) P50, (b) P70, and (c) P100. The vegetation type is coniferous tree and the soil type is loam. The amount of upward soil water diffusion (abbreviated to upward diffusion), through a horizontal cross-section which is located 0.5 m below the root zone bottom, is calculated. The dashed green line indicates the root zone depth (i.e., 5 m). The differences between HR and no-HR experiments are plotted by using a secondary *y* axis (note: the ordinates for the differences are reversed for clarity).

deeper than about 2.5 m, and gets much larger when the GWT becomes deeper than 7 m. When the GWT lies within the shallow GWTD range, HR makes the transport of soil water to the shallow root zone possible and thus, the daytime root uptake is insensitive to the three different precipitation conditions. But when the GWT lies within the intermediate range, the difference in the daytime uptake starts to increase. When the GWT is lowered into the deep range, soil water in the shallow root zone is controlled by the available precipitation, and the differences among the three precipitation conditions are amplified. Thus, the higher the precipitation, the greater the daytime root uptake is. Figures 10d–10f show that the daytime root uptake in the deep root zone is, on the other hand, higher under drier precipitation conditions when the GWT is at about 3–6 m, illustrating again the important role that deep roots play in supporting plant transpiration under dry precipitation conditions.

A comparison of daytime root uptake between the shallow root zone (Figure 10, first row) and deep root zone (Figure 10, second row) clearly shows that the major daytime uptake by roots occurs in the shallow root zone for all three precipitation conditions, as it is where the major root mass concentrates. Interactions between the two root zones are also clearly demonstrated in Figure 10 exhibiting similar behaviors as discussed in section 4.4.

Taking together, impacts by the precipitation conditions on the contribution of HR are explained.

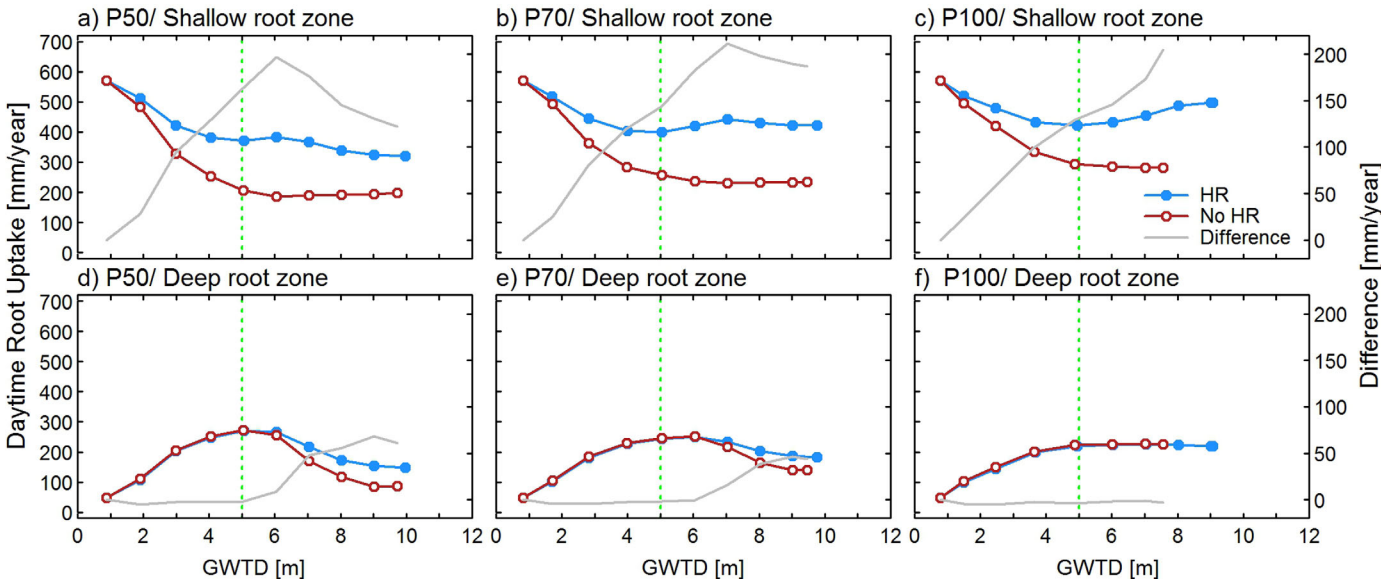

Figure 10. Comparisons of daytime root uptake–GWTD relationships between HR and no-HR experiments for two parts of the root zone ((top row) Shallow root zone and (bottom row) Deep root zone) and three precipitation conditions ((a and d) P50, (b and e) P70, and (c and f) P100). The vegetation type is coniferous tree and the soil type is loam. The differences between HR and no-HR experiments are plotted by using a secondary *y* axis. The dashed green line indicates the root zone depth (i.e., 5 m).

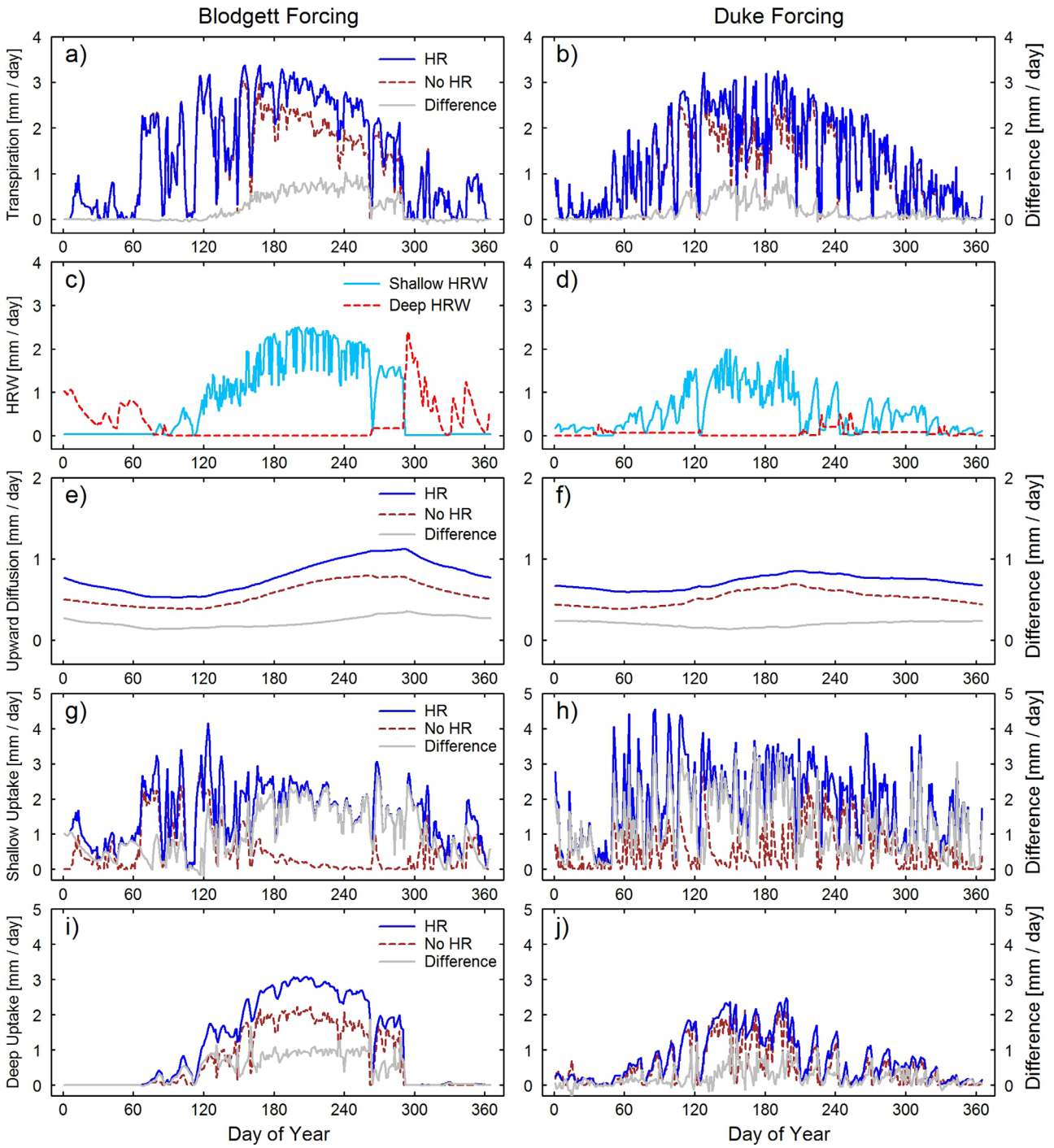

Figure 11. Modeled daily time series of hydrological processes using the forcing input based on the forcing data of (left column) the Blodgett site or (right column) the Duke site: (1) (a and b) plant transpiration, (2) (c and d) hydraulically redistributed water (HRW) in the shallow root zone and the deep root zone, (3) (e and f) upward diffusion of soil water through a horizontal cross-section 0.5 m below the root zone bottom, (4) (g and h) daytime root uptake in the shallow root zone, and (5) (i and j) daytime root uptake in the deep root zone. The results of both HR and no-HR experiments are shown, and the differences between HR and no-HR experiments are plotted by using a secondary *y* axis (except Figures 11c and 11d, where only the results of HR experiments are shown). For all the experiments, the vegetation type is coniferous tree, the soil type is loam, the precipitation condition is P50, and the maximum groundwater table depth (GWTD) is 6 m.

5. Impact of Climate Type

Impacts of HR on the transpiration–GWTD relationship curves are also affected by the characteristics of the climate type, such as different patterns of the temporal distribution of precipitation over the four seasons of

a year. The two precipitation temporal patterns considered at the Duke Forest site and the Blodgett Forest site are different (see Figure 2) as illustrated earlier. The potential transpiration is 670 mm/yr for the former, and 740 mm/yr for the latter. Impacts of the climate type are only investigated in a limited way in this study. We consider a soil column with a maximum GWTD of 6 m under dry precipitation conditions. The vegetation type used is tree and the soil type is loam. Since the results between the Blodgett site and the Duke site on transpiration, HRW, upward diffusion, and daytime root uptake exhibit similar variation patterns and behaviors as those discussed and shown in Figures 7–10, their plots are not shown. Rather we show here the variations of these quantities in time series which are summarized in Figure 11.

For the temporal variation in transpiration, the first row in Figure 11 shows that transpiration is promoted by HR over a long dry summer time period (i.e., from day 170 to day 285) at the Blodgett site, while it is promoted by HR only over some short dry time periods at the Duke site.

As for the HRW, the second row in Figure 11 shows that the HRW in the shallow root zone concentrates in the dry summer under the Blodgett climate type, but appears in most of the 12 months under the Duke climate type. On the other hand, HRW in the deep root zone concentrates in the wet season under the Blodgett climate type, and appears only in several months under the Duke climate type. At the Blodgett site, the concentrated precipitation in the wet season enhances the downward HR and contributes to the larger deep root zone HRW amounts during the wet season.

Regarding the upward soil water diffusion, the third row in Figure 11 shows that the variation of upward soil water diffusion at the daily scale is affected by climate types in both the HR and no-HR scenarios. A drier root zone causes larger water-potential gradient from groundwater to the root zone and thus promote more upward soil water diffusion. Therefore, the upward diffusion amount generally increases in dry seasons and decreases in wet seasons.

The temporal variation of the daytime root uptake is summarized, respectively, in fourth (shallow root) and fifth (deep root) rows in Figure 11. It shows that the daytime root uptake in the deep root zone has different temporal distributions under the two climate types. For the Blodgett case, daytime uptake by deep roots is significant in the dry summer and negligible in the wet winter. For about 3 months of the dry summer, daytime uptake by deep roots is higher than that by shallow roots. This indicates that deep roots play a more significant role in dry seasons. For the Duke case, daytime uptake by deep roots appears in most of the months of the year and is almost always lower than the daytime uptake by the shallow roots. This indicates that the shallow roots play a more important role throughout the year if the temporal distribution of precipitation is relatively uniform.

Even for an investigation of limited scope as presented here, results obtained and summarized in Figure 11 show that the temporal patterns in forcing condition have a significant impact. The preceding discussions demonstrate that the HR mechanism as presented so far also facilitates the understanding of the temporal variation trend observed.

6. Conclusions

In this study, the role of hydraulic redistribution (HR) in the interplay between plant transpiration and groundwater dynamics is investigated by using the Variable Infiltration Capacity Plus (VIC+) land surface model. Impacts of HR on modulating available soil moisture during the initial stage of a dry period and on linking the surface and subsurface processes are analyzed under the steady state conditions achieved at an annual scale in which the seasonal cycle of each year repeats. Conditions under which surface and subsurface processes become decoupled are identified. Important findings from this study are summarized below.

1. HR's impacts on the plant transpiration–GWTD relationship can be explained by the soil moisture state in the root zone. GWT affects the soil moisture state around the plant root zone which, in turn, determines the mode of transpiration.
2. Plants with deep roots can play a significant role in adjusting available soil moisture at the initial stage of an extended dry period and lessen the impacts of the water shortage by redistributing water to the surface through the upward HR and the soil water diffusion processes. This effectively expands the range of GWTD over which transpiration is maintained at a high rate (i.e., at a pseudo energy-limited rate). Thus, during this time period, plants do not experience the dry condition. After this initial stage, effects of the dry conditions set in and plant transpiration transits to a low rate (i.e., in the transition region). Plant

transpiration at this time is controlled by the moderate soil moisture state in the root zone. As the dry period prolongs and becomes severe, plant transpiration can only be sustained at a very low rate controlled by the precipitation. Without HR, plants would experience dry condition much earlier and for a longer period of time. Thus, the transpiration cycle of the plants under the dry climate conditions would be projected incorrectly without considering HR.

3. HR serves as an important linkage between the surface (e.g., transpiration) and subsurface processes (e.g., upward diffusion and GWT dynamics) when the GWT is within the distance that can be reached by diffusion below the root zone bottom. The upward HR process, assist by the upward diffusion process, makes the groundwater resource available to the shallower soil layer for plant utilization. On the other hand, the downward HR process makes it more effectively to transfer the soil water of the shallow root zone, after rainfall events, to the deep root zone for storage or to recharge the groundwater.
4. For plants with deep roots even at a small percentage, HR significantly enlarges the pseudo energy-limited region under dry precipitation conditions and shrinks the transitional region, while the water-limited region remains about the same as that with no-HR. The HR contributed increase in transpiration varies with the GWTD (grey lines in Figure 3). The largest increase occurs when the GWT lies in the vicinity of the root zone bottom (e.g., between 4 and 6 m in Figure 3a) because of a combined effect resulted from HR and the upward diffusion process. This can be observed by viewing together the grey lines in Figure 3, the shallow HRW (light blue lines) in Figure 4, the differences in upward diffusion (grey lines) in Figure 5, and the uptake differences in the shallow root zone (grey lines) in Figure 6. For the tree type vegetation under the dry precipitation condition, for example, HR can promote transpiration by 15%–30% from loamy sand to clay when the GWT is around the root zone bottom (Figures 3a–3c).
5. Results from the no-HR experiments of this study affirm the finding of the previous no-HR studies [e.g., *Maxwell and Kollet*, 2008] on the presence of the three regions under some situations, in the transpiration–GWTD relationship. With HR included, this study shows that the pseudo energy-limited region in the transpiration–GWTD relationship is enlarged.
6. This study also shows that the transpiration–GWTD relationships are affected by climates and by the characteristics of the meteorological forcing data. Even though this part of work is limited, the same mechanism as laid out appears to apply.

In summary, results from this study show that HR can affect the water cycle in the root zone and the region right below the root zone, enhance the utilization of groundwater by plants, and promote plant transpiration, especially under dry precipitation conditions. It is, therefore, very important to adequately represent HR in land surface models and in the coupled land-atmosphere models, and to consider the role of HR when studying the interactions among groundwater, the land surface, and the atmosphere in the soil-plant-atmosphere continuum.

The numerical experiments of this study are conducted on homogenous soil columns. This modeling strategy has its advantages and disadvantages. It provides a setting that facilitates the exploration and interpretation of the mechanism underlying HR, and it complements watershed-based studies. The disadvantage is that the soil profiles are idealized and the assumption of homogeneous soil is different from the natural soil profile. The subsurface heterogeneity could have large effect on the interplay among HR, groundwater, and the land surface processes. In addition, this study does not consider the plant physiology as the root structures are prescribed and do not change. When roots are stressed or in a phase recovering from stress, their changes in physiology could affect root functions and alter plant transpiration characteristics. These topics certainly deserve further investigations in the watershed-scale or region-scale modeling studies in which HR and the unconfined aquifer are represented.

Table A1. Values of Vegetation Parameters

Vegetation Type	Extinction Coefficient (β) of Equation (4)	Live Fine Root Area Index (LFRAI) ($m^2 \cdot m^{-2}$)	Maximum Root Depth (m)
Coniferous tree	0.98	11.0	5
Shrub	0.95	11.6	4
Grass	0.94	79.1	2

Appendix A: Parameter Values

The vegetation parameter values used in this study are shown in the Table A1. The extinction coefficient (β) of the equation (4) and the live fine root area index are from *Jackson et al.* [1997].

Table A2. Values of Soil Parameters

Soil Type	θ_r	θ_s	α (m^{-1})	n	K_{sat} ($m \cdot s^{-1}$)
Loam	0.061	0.399	1.11	1.47	1.39×10^{-6}
Loamy sand	0.049	0.390	3.48	1.75	1.22×10^{-5}
Clay	0.098	0.459	1.50	1.25	1.71×10^{-6}

For unsaturated soil, the soil water content (θ) is linked to the soil water potential (ψ_s) through the following formula [*van Genuchten*, 1980]:

$$\theta(\psi_s) = \theta_r + (\theta_s - \theta_r) \cdot \left[1 + (\alpha|\psi_s|)^n\right]^{\frac{1-n}{n}} \tag{A1}$$

where θ_r ($m^3\ m^{-3}$) is the residual soil water content; θ_s ($m^3\ m^{-3}$) is the saturated soil water content; parameters α (m^{-1}) and n are experimentally determined for different soil types.

The soil hydraulic conductivity (K_s) is predicted from the soil water potential (ψ_s) by using the following formula [*van Genuchten*, 1980]:

$$K_s(\psi_s) = K_{sat} \cdot \left[1 + (\alpha|\psi_s|)^n\right]^{\frac{1-n}{2n}} \cdot \left\{1 - (\alpha|\psi_s|)^{n-1} \cdot \left[1 + (\alpha|\psi_s|)^n\right]^{\frac{1-n}{n}}\right\}^2 \tag{A2}$$

where K_{sat} ($m^2 \cdot s^{-1} \cdot Pa^{-1}$) is the hydraulic conductivity of saturated soil; parameters α and n are the same as those of equation (A1).

The soil parameter values used in this study are shown in the Table A2. These values are from the database of the ROSETTA model maintained by the Agricultural Research Service of United States Department of Agriculture.

Acknowledgments
The authors are thankful to the three reviewers, the Editor, and the Associate Editor for their valuable comments and suggestions. We thank Maoyi Huang for the helpful discussions. We also thank the Center for Simulation and Modeling of the Swanson School of Engineering at the University of Pittsburgh for providing computing resources for this work. The data of the AmeriFlux site used in this study can be obtained freely from the AmeriFlux web site (http://ameriflux.ornl.gov/). The AmeriFlux research is supported by the U.S. Department of Energy and National Aeronautics and Space Administration. The data used to generate the figures in this paper can be accessed by contacting the corresponding author. This work was partially supported by the DOE grant DEFG0208ER64586 and by the NOAA grant NA09OAR4310168 to the University of Pittsburgh. The second author also acknowledges the support from the William Kepler Whiteford Professorship from the University of Pittsburgh.

References

Amenu, G. G., and P. Kumar (2008), A model for hydraulic redistribution incorporating coupled soil-root moisture transport, *Hydrol. Earth Syst. Sci.*, *12*(1), 55–74.
Caldwell, M. M., and J. H. Richards (1989), Hydraulic lift: Water efflux from upper roots improves effectiveness of water uptake by deep roots, *Oecologia*, *79*(1), 1–5, doi:10.1007/BF00378231.
Caldwell, M. M., T. E. Dawson, and J. H. Richards (1998), Hydraulic lift: Consequences of water efflux from the roots of plants, *Oecologia*, *113*(2), 151–161, doi:10.1007/s004420050363.
Chen, X., and Q. Hu (2004), Groundwater influences on soil moisture and surface evaporation, *J. Hydrol.*, *297*, 285–300, doi:10.1016/j.jhydrol.2004.04.019.
Cherkauer, K. A., and D. P. Lettenmaier (1999), Hydrologic effects of frozen soils in the upper Mississippi River basin, *J. Geophys. Res.*, *104*(D16), 19,599–19,610, doi:10.1029/1999JD900337.
Cherkauer, K. A., and D. P. Lettenmaier (2003), Simulation of spatial variability in snow and frozen soil, *J. Geophys. Res.*, *108*(D22), 8858, doi:10.1029/2003JD003575.
Condon, L. E., R. M. Maxwell, and S. Gangopadhyay (2013), The impact of subsurface conceptualization on land energy fluxes, *Adv. Water Resour.*, *60*, 188–203, doi:10.1016/j.advwatres.2013.08.001.
Davis, T. W., and X. Liang (2013), The potential use of soil moisture sensors for observing hydraulic redistribution characteristics, *J. Water Resour. Hydraul. Eng.*, *2*(3), 84–91.
Dawson, T. E. (1993), Hydraulic lift and water use by plants: Implications for water balance, performance and plant-plant interactions, *Oecologia*, *95*(4), 565–574.
Dawson, T. E. (1996), Determining water use by trees and forests from isotopic, energy balance and transpiration analyses: The roles of tree size and hydraulic lift, *Tree Physiol.*, *16*(1-2), 263–272, doi:10.1093/treephys/16.1-2.263.
Fan, Y., G. Miguez-Macho, C. P. Weaver, R. Walko, and A. Robock (2007), Incorporating water table dynamics in climate modeling: 1. Water table observations and equilibrium water table simulations, *J. Geophys. Res.*, *112*, D10125, doi:10.1029/2006JD008111.
Ferguson, I. M., and R. M. Maxwell (2010), Role of groundwater in watershed response and land surface feedbacks under climate change, *Water Resour. Res.*, *46*, W00F02, doi:10.1029/2009WR008616.
Franchini, M., and M. Pacciani (1991), Comparative analysis of several conceptual rainfall-runoff models, *J. Hydrol.*, *122*(1-4), 161–219, doi:10.1016/0022-1694(91)90178-K.
Gale, M. R., and D. F. Grigal (1987), Vertical root distributions of northern tree species in relation to successional status, *Can. J. For. Res.*, *17*(8), 829–834.
Gou, S., and G. Miller (2014), A groundwater–soil–plant–atmosphere continuum approach for modelling water stress, uptake, and hydraulic redistribution in phreatophytic vegetation, *Ecohydrology*, *7*(3), 1029–1041, doi:10.1002/eco.1427.
Gutowski, W. J., C. J. Vörösmarty, M. Person, Z. Ötles, B. Fekete, and J. York (2002), A Coupled Land-Atmosphere Simulation Program (CLASP): Calibration and validation, *J. Geophys. Res.*, *107*(D16), doi:10.1029/2001JD000392.
Huang, M., and X. Liang (2006), On the assessment of the impact of reducing parameters and identification of parameter uncertainties for a hydrologic model with applications to ungauged basins, *J. Hydrol.*, *320*(1-2), 37–61, doi:10.1016/j.jhydrol.2005.07.010.
Jackson, R. B., H. A. Mooney, and E. D. Schulze (1997), A global budget for fine root biomass, surface area, and nutrient contents, *Proc. Natl. Acad. Sci. U. S. A.*, *94*(14), 7362–7366.

Kollet, S. J., and R. M. Maxwell (2008), Capturing the influence of groundwater dynamics on land surface processes using an integrated, distributed watershed model, *Water Resour. Res.*, *44*, W02402, doi:10.1029/2007WR006004.
Landsberg, J. J., and N. D. Fowkes (1978), Water movement through plant roots, *Ann. Bot.*, *42*(179), 493–508.
Lee, J.-E., R. S. Oliveira, T. E. Dawson, and I. Fung (2005), Root functioning modifies seasonal climate, *Proc. Natl. Acad. Sci. U. S. A.*, *102*(49), 17,576–17,581, doi:10.1073/pnas.0508785102.
Leung, L., M. Huang, Y. Qian, and X. Liang (2011), Climate–soil–vegetation control on groundwater table dynamics and its feedbacks in a climate model, *Clim. Dyn.*, *36*(1), 57–81, doi:10.1007/s00382-010-0746-x.
Lhomme, J. P., A. Rocheteau, J. M. Ourcival, and S. Rambal (2001), Non-steady-state modelling of water transfer in a Mediterranean evergreen canopy, *Agric. For. Meteorol.*, *108*(1), 67–83.
Li, H., M. Huang, M. S. Wigmosta, Y. Ke, A. M. Coleman, L. R. Leung, A. Wang, and D. M. Ricciuto (2011), Evaluating runoff simulations from the Community Land Model 4.0 using observations from flux towers and a mountainous watershed, *J. Geophys. Res.*, *116*, D24120, doi:10.1029/2011JD016276.
Liang, X., and Z. Xie (2001), A new surface runoff parameterization with subgrid-scale soil heterogeneity for land surface models, *Adv. Water Resour.*, *24*(9–10), 1173–1193, doi:10.1016/S0309-1708(01)00032-X.
Liang, X., and Z. H. Xie (2003), Important factors in land-atmosphere interactions: surface runoff generations and interactions between surface and groundwater, *Glob. Planet. Change*, *38*(1–2), 101–114.
Liang, X., D. P. Lettenmaier, E. F. Wood, and S. J. Burges (1994), A simple hydrologically based model of land surface water and energy fluxes for general circulation models, *J. Geophys. Res.*, *99*(D7), 14,415–14,428, doi:10.1029/94JD00483.
Liang, X., D. P. Lettenmaier, and E. F. Wood (1996a), One-dimensional statistical dynamic representation of subgrid spatial variability of precipitation in the two-layer variable infiltration capacity model, *J. Geophys. Res.*, *101*(D16), 21,403–21,422, doi:10.1029/96JD01448.
Liang, X., E. F. Wood, and D. P. Lettenmaier (1996b), Surface soil moisture parameterization of the VIC-2L model: Evaluation and modification, *Global Planet. Change*, *13*, 195–206.
Liang, X., E. F. Wood, and D. P. Lettenmaier (1999), Modeling ground heat flux in land surface parameterization schemes, *J. Geophys. Res.*, *104*(D8), 9581–9600, doi:10.1029/98JD02307.
Liang, X., Z. Xie, and M. Huang (2003), A new parameterization for surface and groundwater interactions and its impact on water budgets with the variable infiltration capacity (VIC) land surface model, *J. Geophys. Res.*, *108*(D16), 8613, doi:10.1029/2002JD003090.
Liang, X., J. Guo, and L. R. Leung (2004), Assessment of the effects of spatial resolutions on daily water flux simulations, *J. Hydrol.*, *298*(1–4), 287–310, doi:10.1016/j.jhydrol.2003.07.007.
Liang, X., L. R. Leung, M. Huang, Y. Qian, M. S. Wigmosta, G. B. Matanga, and D. Matthews (2006), PUB Working Group on orographic precipitation, surface and groundwater interactions, and their impacts on water resources, in *Predictions in Ungauged Basins: Promise and Progress*, edited by M. Sivapalan *et al.*, IAHS Publ., vol. 303, pp. 505–515.
Lubczynski, M. (2009), The hydrogeological role of trees in water-limited environments, *Hydrogeol. J.*, 247–259, doi:10.1007/s10040-008-0357-3.
Luo, X., X. Liang, and H. R. McCarthy (2013), VIC+ for water-limited conditions: A study of biological and hydrological processes and their interactions in soil-plant-atmosphere continuum, *Water Resour. Res.*, *49*, 7711–7732, doi:10.1002/2012WR012851.
Maxwell, R. M. (2010), Infiltration in arid environments: Spatial patterns between Subsurface heterogeneity and water-energy balances, *Vadose Zone J.*, *9*(4), 970–983, doi:10.2136/vzj2010.0014.
Maxwell, R. M., and S. J. Kollet (2008), Interdependence of groundwater dynamics and land-energy feedbacks under climate change, *Nat. Geosci.*, *1*(10), 665–669, doi:10.1038/ngeo315.
Maxwell, R. M., and N. L. Miller (2005), Development of a Coupled Land Surface and Groundwater Model, *J. Hydrometeorol.*, *6*(3), 233–247, doi:10.1175/JHM422.1.
Mendel, M., S. Hergarten, and H. J. Neugebauer (2002), On a better understanding of hydraulic lift: A numerical study, *Water Resour. Res.*, *38*(10), 1183, doi:10.1029/2001WR000911.
Miguez-Macho, G., Y. Fan, C. P. Weaver, R. Walko, and A. Robock (2007), Incorporating water table dynamics in climate modeling: 2. Formulation, validation, and soil moisture simulation, *J. Geophys. Res. Atmospheres*, *112*(D13), D13108, doi:10.1029/2006JD008112.
Niu, G.-Y., Z.-L. Yang, R. E. Dickinson, L. E. Gulden, and H. Su (2007), Development of a simple groundwater model for use in climate models and evaluation with Gravity Recovery and Climate Experiment data, *J. Geophys. Res.*, *112*, D07103, doi:10.1029/2006JD007522.
Oliveira, R. S., T. E. Dawson, S. S. O. Burgess, and D. C. Nepstad (2005), Hydraulic redistribution in three Amazonian trees, *Oecologia*, *145*(3), 354–363, doi:10.1007/s00442-005-0108-2.
Quijano, J. C., and P. Kumar (2015), Numerical simulations of hydraulic redistribution across climates: The role of the root hydraulic conductivities, *Water Resour. Res.*, *51*, 8529–8550, doi:10.1002/2014WR016509.
Rihani, J. F., R. M. Maxwell, and F. K. Chow (2010), Coupling groundwater and land surface processes: Idealized simulations to identify effects of terrain and subsurface heterogeneity on land surface energy fluxes, *Water Resour. Res.*, *46*(12), W12523, doi:10.1029/2010WR009111.
Ryel, R. J., M. M. Caldwell, C. K. Yoder, D. Or, and A. J. Leffler (2002), Hydraulic redistribution in a stand of Artemisia tridentata: Evaluation of benefits to transpiration assessed with a simulation model, *Oecologia*, *130*(2), 173–184, doi:10.1007/s004420100794.
Soylu, M. E., E. Istanbulluoglu, J. D. Lenters, and T. Wang (2011), Quantifying the impact of groundwater depth on evapotranspiration in a semi-arid grassland region, *Hydrol. Earth Syst. Sci.*, *15*(3), 787–806, doi:10.5194/hess-15-787-2011.
van Genuchten, M. T. (1980), A closed-form equation for predicting the hydraulic conductivity of unsaturated soils, *Soil Sci. Soc. Am. J.*, *44*(5), 892–898.
Walker, J. P., and P. R. Houser (2004), Requirements of a global near-surface soil moisture satellite mission: Accuracy, repeat time, and spatial resolution, *Adv. Water Resour.*, *27*(8), 785–801, doi:10.1016/j.advwatres.2004.05.006.
Wang, G. (2011), Assessing the potential hydrological impacts of hydraulic redistribution in Amazonia using a numerical modeling approach, *Water Resour. Res.*, *47*, W02528, doi:10.1029/2010WR009601.
Yeh, P. J.-F., and E. A. B. Eltahir (2005), Representation of water table dynamics in a land surface scheme. Part I: Model development, *J. Clim.*, *18*(12), 1861–1880, doi:10.1175/JCLI3330.1.
York, J. P., M. Person, W. J. Gutowski, and T. C. Winter (2002), Putting aquifers into atmospheric simulation models: An example from the Mill Creek Watershed, northeastern Kansas, *Adv. Water Resour.*, *25*(2), 221–238, doi:10.1016/S0309-1708(01)00021-5.
Zampieri, M., E. Serpetzoglou, E. N. Anagnostou, E. I. Nikolopoulos, and A. Papadopoulos (2012), Improving the representation of river–groundwater interactions in land surface modeling at the regional scale: Observational evidence and parameterization applied in the Community Land Model, *J. Hydrol.*, *420–421*, 72–86, doi:10.1016/j.jhydrol.2011.11.041.